

Reviewed Preprint

v1 • November 25, 2025

Not revised

Reviewed Preprint

v2 • April 14, 2026

Revised by authors

✉ For correspondence:

malfatti@disroot.orgklas.kullander@igp.uu.se

* equal contribution,

† Present address: Department of Biology, University of Maryland, College Park, United States

deceased 2022

Competing interests: No competing interests declared**Funding:** See [page 23](#)**Reviewing editor:** Jun Ding, Stanford University, United States

© 2025, Malfatti et al. This article is distributed under the terms of the

[Creative Commons Attribution](#)[License](#), which permits unrestricted use and redistribution provided that the original author and source are credited.

Increased layer 5 Martinotti cell excitation reduces pyramidal cell population plasticity and improves learned motor execution

Thawann Malfatti^{1,*} ✉, Anna Velica^{1,*}, Jéssica Winne^{1,2,†}, Barbara Ciralli^{1,2}, Katharina Henriksson¹, George Nascimento^{2,#}, Richardson Leao², Klas Kullander¹ ✉¹Department of Immunology, genetics and pathology, Uppsala University, Uppsala, Sweden • ²Brain Institute, Federal University of Rio Grande do Norte, Natal, Brazil

eLife Assessment

This **valuable** study addresses a critical question regarding the role of a subpopulation of cortical interneurons (Chrna2-expressing Martinotti cells) in motor learning and cortical dynamics. However, despite the inclusion of interesting behavioral and imaging data, significant limitations remain, even after revision, in the design of the motor learning task and the associated data analyses. As a result, the presented data are **incomplete** to support the central conclusions.

<https://doi.org/10.7554/eLife.109286.2.sa3>

Abstract

During motor activity and motor learning, pyramidal cells in the motor cortex receive inputs from local interneurons as well as deeper structures. Layer 5 pyramidal cells in the primary motor cortex then feed commands to spinal circuits for motor execution. The genetic ablation of layer 5 Chrna2 Martinotti cells, which selectively target pyramidal tract pyramidal cells, resulted in disturbed fine motor functions. Using calcium imaging combined with chemogenetics, we show that activation of layer 5 Chrna2 Martinotti cells during training increases pyramidal cell tuning, changes responses temporal patterns and decreases assembly reconfiguration, while not affecting motor learning success rates. However, in mice that had already learned a reach-and-grasp (prehension) task, Chrna2 Martinotti cell activation resulted in improved prehension and increased power in low theta and high gamma bands of local field potentials in the motor cortex. This work indicates that activation of Chrna2 Martinotti cells reduces pyramidal cell assembly plasticity during learning, possibly facilitating already acquired motor skills.

Introduction

Refined control of limb movement is crucial to perform essential behaviors such as building shelter, reaching for objects and exploring food. To initiate a voluntary movement, information is relayed from processed sensory information and command centers to circuits in the motor cortex, where the intended motor sequence is processed. The primary motor cortex (M1), which processes motor plans involving proximal and distal joints [1], delivers commands to spinal cord neurons to execute motor behaviors [2]. Motor plasticity continuously shapes and refines the neural circuits underlying motor control, ultimately influencing the execution of motor tasks in diverse contexts and conditions [3]. How the cortex is involved in motor learning and the execution of learned movements is still under debate. Most studies agree that cortical processing is necessary for the initiation of a learned motor sequence [4, 5, 6], but it remains unclear whether cortical processing is necessary for its execution. For example, a study used lesions and a lever pressing task to show

that the rodent motor cortex is required for learning, but not for the execution of movements [7]. However, the use of optogenetic mid-movement activation of local inhibitory interneurons in the motor cortex could pause the execution of a learned movement, providing contradictory data [8]. Cortical excitatory and inhibitory interneurons serve as an interface between sensory inputs and motor commands and can thus provide entry points for the congregation of direct sensory input and processed information from the prefrontal cortex, to achieve the most purposeful movement at any given moment. Identifying the function and connectivity of specific interneuron populations within M1 is an important step towards disentangling the neuronal circuits that control and modulate motor function.

Martinotti cells (MCs) are inhibitory interneurons, mainly found in neocortical layer 3 and 5 [9], typically express the neuropeptide somatostatin (SST), and project to layer 1 where they form synapses onto the distal dendrites of cortical pyramidal cells [PCs; 10]. There are several studies investigating the connectivity and functional role of SST-expressing interneurons [11, 12, 13, 14, 15]. However, in the cortex, SST is expressed in a variety of diverse interneuron populations including large basket cells, double-bouquet cells, long-range GABAergic projection cells, bitufted cells, fanning-out MCs and T-shaped MCs [9, 16, 17]. In fact, only around 50% of SST interneurons are MCs [18] and MCs are found in all cortical layers except for layer 1 [19]. Recently it has been shown that more specific genetic markers can subdivide SST interneurons and MCs into subtypes that reside in different cortical layers and exhibit different morphologies and axonal projection patterns [20, 21], resulting in different layer specific functional properties [22, 16]. Indeed, a motor learning study has suggested that each cortical layer operates under unique constraints reflective of its specialized function [23].

In mice, a subset of MCs (herein referred to as *Ma2* cells) located in layer 5b, expressing the cholinergic receptor nicotinic alpha 2 subunit (*Chrna2*), send inhibitory projections selectively to thick-tufted type A pyramidal tract PC where they can reset and synchronize PC activity in a frequency-dependent manner [24, 21]. These findings suggest that *Ma2* cells are important for coordinated pyramidal tract PC activity, which is involved in top-down control of subcortical structures. However, how *Ma2* cells might influence PC activity to learn and execute purposeful motor behaviors is not understood. To probe the possible role of *Ma2* cells in motor processing, we evaluated skilled forelimb motor learning and execution in a prehension task during chemogenetic activation of *Ma2* cells, while simultaneously recording layer 5 PC activity using calcium imaging. We found that increased excitation of *Ma2* cells reduced plasticity in PC assemblies during learning, although learning efficiency was unaffected. Here, “assemblies” refer to functionally defined groups of pyramidal cells with temporally correlated activity patterns and are thought to represent cooperative network units underlying information processing. In contrast, motor performance of an already acquired skill was improved, suggesting that layer 5 Martinotti cells are required for cortical plasticity and motor execution.

Materials and methods

Animals

All animal procedures were approved by the local animal research ethical committee (Uppsala djurförsöksetiskanämnd) and followed the Swedish Animal Welfare Act (Svensk författningssamling (SFS) 2018:1192), The Swedish Animal Welfare Ordinance (SFS 2019:66) and the Regulations and general advice for laboratory animals (SJVFS 2019:9, Saknr L 150). Ethical permit number: 5.8.18-08463/2018, 5.8.18-08464/2018 and 5.8.18-07526/2023. *Chrna2*-Cre mice, produced and bred in our own facility [25], were crossed with either C57BL/6J (Taconic, Denmark), GT(ROSA)26Sortm14(CAG-tdTomato)Hze [RRID:IMSR_JAX:007914 [↗](#); 26] or GT(ROSA)26Sortm1.1(CAG-EGFP)Fsh/Mmjjax [RRID:MMRRC_032037-JAX [↗](#); 27] mice and the offspring were genotyped in house for the presence of the *Chrna2*-Cre allele and/or the tdTomato allele and the EGFP allele. The following primers were used: *Chrna2*-Cre 5'-gacagccattttctgcttc-3' (forward) and 5'-aggcaaatttgggtacgg-3' (reverse); tdTomato 5'-ctgttctgtacggcatgg-3' (forward) and 5'-ggcattaaagcagcgtatcc-3' (reverse); EGFP 5'-gacgtaaaccgccacaagttc-3' (forward) and 5'-

gtcttctgct-3' (reverse). The *Chrna2-Cre*, *td-Tomato* and *EGFP* allele were kept heterozygous. Mice were housed with littermates in approximately 501 cm² individually ventilated cages (up to 5 mice/cage) with bedding and enrichment (a carton house and paper tissues), kept in a 12-h light on/light off cycle (6 a.m.–6 p.m.), and maintained at 21 ± 2 °C with a humidity of 45-64%. Mice were provided food (diet pellets, Scanbur, Sweden) and tap water ad libitum, except for when food was restricted for behavioral testing (see single pellet prehension task and pasta handling task further down). After lens or electrode implant surgery, mice were housed individually to decrease risk of implant detachment. Mice were 6-25 weeks old at the start of experiments. *Chrna2-Cre^{tg/wt}* and *Chrna2-Cre^{wt/wt}* (*Cre*-negative littermates designated “controls”) were used. *Chrna2-Cre^{tg/wt}-tdTomato^{lx/wt}* mice (and *Cre*-negative littermates, *Chrna2-Cre^{wt/wt}-tdTomato^{lx/wt}*; controls) were only used for experiments with *Cre*-dependent caspase3-induced apoptosis. Female mice were used in the behavioral experiments, except for in the miniscope recordings in which male mice were used. Throughout the paper, control mice refer to *Cre*-negative littermates that have received the same treatment as *Cre*-positive mice.

Viral injections

Mice were sedated with 1-4% Isoflurane (Baxter). Analgesia was given subcutaneously; 2 mg/kg bupivacaine (Marcain, AstraZeneca), 5 mg/kg carprofen (Norocarp vet, N-vet or Rimadyl Biovis vet) and 0.1 mg/kg buprenorphine (Vetergesic vet, Ceva). A midline incision was made in the scalp, muscles and periosteum were removed using 3% hydrogen peroxide (Sigma-Aldrich) and a hole (1 mm in diameter) was drilled at the site of injection (coordinates relative to bregma: AP 0.8 mm, ML 1.5 mm and DV -1.3 mm) with a hand-held drill. The injection coordinates targeted the forelimb area of the M1. The injection coordinates were chosen based on the Mouse Brain Atlas [28], as well as previous studies mapping the motor cortex [29, 30]. Viral vectors (for more information see below for each experiment) were injected using a 10 µl Nanofil Hamilton syringe (WPI, USA) mounted on a stereotaxic frame. Ten minutes post injection the needle was slowly withdrawn from the brain and the wound was stitched with resorbable sutures (Vicryl rapide, Ethicon, 6-0). Mice were then left to recover for 2-4 weeks before any behavioral experiments were initiated. Viral transduction was confirmed by post-hoc histological analysis of brain sections.

For *Cre*-dependent caspase3-induced apoptosis, 14 female mice (7 *Chrna2-Cre^{tg/wt}-tdTomato^{lx/wt}*; 7 *Chrna2-Cre^{wt/wt}-tdTomato^{lx/wt}*) were injected bilaterally with 750 nl of AAV5-FLEX-TACASP3-TEVP (Addgene viral prep # 45580-AAV5, viral titer: 4.6 × 10¹² VG/ml) at a speed of 100 nl/min and were used for behavioral experiments. Two additional mice were injected unilaterally in order to check the percentage of neuronal ablation comparing the injected to the non-injected side.

For chemogenetic activation during local field potential (LFP) recordings, 14 female mice (7 *Chrna2-Cre^{tg/wt}*; 7 *Chrna2-Cre^{wt/wt}*) were injected bilaterally with 300 nl of AAV9-hSyn-DIO-hM3Dq-mCherry (Addgene viral prep # 44361-AAV9, viral titer 2.3 × 10¹³ GC/ml) diluted in 300 nl sterile saline (9 mg/ml, Fresenius Kabi, Sweden) at a speed of 200 nl/min.

For repetitive chemogenetic activation during training of the single pellet prehension task, 21 mice (10 *Chrna2-Cre^{tg/wt}*; 11 *Chrna2-Cre^{wt/wt}*) were injected bilaterally with 300 nl of AAV9-hSyn-DIO-hM3Dq-mCherry diluted in 300 nl sterile saline (9 mg/ml, Fresenius Kabi, Sweden) at a speed of 200 nl/min.

For calcium imaging of pyramidal cell activity, 8 mice (5 *Chrna2-Cre^{tg/wt}*; 3 *Chrna2-Cre^{wt/wt}*) were first injected bilaterally with 300 nl of AAV9-hSyn-DIO-hM3Dq-mCherry diluted in 300 nl sterile saline (9 mg/ml, Fresenius Kabi, Sweden) at a speed of 200 nl/min. One week post injection, the mice were injected unilaterally in the right hemisphere with 600 nl of AAV9-CamKII-GCaMP6f-WPRE-SV40 (Addgene viral prep # 100834-AAV9), at a speed of 200 nl/min. One week post-injection of AAV9-CamKII-GCaMP6f-WPRE-SV40, the mice underwent surgery for lens implantation (see Lens implantation below).

Electrode array assembly and implantation

For LFP experiments, mice were injected with AAV9-hSyn-DIO-hM3Dq-mCherry (see viral injections above) bilaterally three weeks before electrode implantation surgery. Tungsten insulated wires of 35 μ m diameter (impedance 100-400 k Ω , California Wires Company) were used to manufacture 2 \times 5 arrays of 10 tungsten wire electrodes. The wires were assembled to a 16 channel custom made printed circuit board and fitted with an Omnetics connector (NPD-18-VV-GS). Electrode wires were spaced 200 μ m and the array was implanted into the right hemisphere of the M1. Surgery preparation was performed as described for viral injection, and four small craniotomies were done in a square at coordinates AP 0.70 mm, ML 1.25 mm; AP 0.70 mm, ML 2.25 mm; AP 1.0 mm, ML 1.25 mm; and AP 1.0 mm, ML 2.25 mm; to make a cranial window were the electrodes were slowly inserted at DV -1.30 mm. Four additional craniotomies were drilled for the placement of anchoring screws (AgnThos, MCS1 \times 2), where the screw placed over the cerebellum served as reference. The electrode implant was fixed to the skull with dental cement (Tetric EvoFlow) around the anchor screws. After surgery, the mice were monitored until awake, housed individually and allowed to recover for one week before recordings.

Lens implantation

The procedure was initially identical to the viral injections, but instead of injecting a virus, a prism lens (CLH type glass, lens diameter 1.0 mm, prism size 1.0 mm, total length of lens+prism 3.68 \pm 0.156 mm, working distance 0.3 mm, enhanced aluminum and SiO₂ protective coating, Go!Foton, USA) combined with a relay GRIN lens (Imaging Focusing Rod Lens, diameter 2.0 mm, working distance at infinity) for recordings of cortical layer 5 was implanted unilaterally using the stereotaxic frame. To implant the prism lenses, the tip of a dissection knife was inserted 0.3 mm into the cortex for three minutes before the lens was lowered into the cortex with the tip 0.3 mm lateral and -0.5 mm dorsoventral to the viral injection coordinates. The lens was fixed to the skull and anchor screws with cyanoacrylate glue (OptiBond, Kerr Dental). Silicon glue (Kwik-Sil, World Precision Instruments) was added to protect the lens from mechanical damage in between experiments. Mice were treated with Enrofloxacin 5 mg/kg (Baytril) for two days pre-surgery and seven days post-surgery. Two to three weeks post implantation the mice were again anesthetized, the scalp incised, and the baseplate (used to attach the miniscope during recordings) was mounted on top of the skull with cyanoacrylate glue. To verify that the prism lens was correctly positioned, we performed post-hoc histological analysis to confirm that it was centered around the cortical layer 5.

Drug preparation

The most commonly used chemogenetic agonist is clozapine-N-oxide (CNO), however, it has been suggested that the main effect on the engineered receptors, after systemically administered CNO, is mediated by back-converted clozapine [CLZ; 31, 32]. Since the conversion rate might differ between individuals [33], we chose to use low dose CLZ for chemogenetic experiments. A stock solution was made from 1 mg of CLZ (Hello Bio, batch E0697-1-1) dissolved in 40 μ l dimethyl sulfoxide (DMSO, Sigma-Aldrich). The stock solution was kept at room temperature for the entire set of experiments. The working solution given to the mice was made fresh daily; 2 μ l of the stock solution were diluted in sterile saline to a final drug concentration of 1 μ g/ml. The mice then received 0.01 mg/kg CLZ intraperitoneally (i.p.).

Single pellet prehension task

The single pellet prehension protocol consisted of handling, habituation and test sessions. The handling and habituation were performed the same way throughout all experiments, while the number of test sessions varied based on the experimental design (see below for more information about each experimental group). During handling, each mouse was placed on the body and hands of the experimenter for five minutes during two consecutive days and sugar pellets (non-pareille, Dr.Oetker) were inserted in the home cages after handling. For habituation, after completed handling, mice were placed inside the test arena for ten minutes and allowed to freely behave

with sugar pellets on the floor of the arena during two consecutive days. The arena consisted of an acrylic rectangular box of dimensions 22 cm x 9 cm x 20.5 cm with a vertical slit (0.5 cm wide) in one of the narrower walls. An elevated (2cm) plate was attached to the outer wall of the arena, 2cm to the right of the slit. On the third day of habituation, mice were presented sugar pellets on a spoon, outside the slit of the arena, which they were allowed to retrieve with their tongues. Following habituation, the mice underwent ten minutes long test sessions every other day. All test sessions were performed after 15-20 hours of food restriction, starting at 5 p.m. the previous day. After the test session, the mice were returned to their homecage with free access to food and water. For all mice, the initial sessions were performed with spoon aided pellet delivery, to make it easier for mice to understand that they should reach for the pellet. The spoon was initially placed closer to the opening of the slit to increase success rate and motivation to perform the test. As the mice reached more, the spoon was gradually moved further away from the slit until it was at the same distance as a fixed position on the plate outside the slit. After the fifth session, the pellet was presented on the fixed position on the plate, instead of on the spoon. The use of a gradually increasing difficulty in the task is needed due to the very challenging position of the plate. The plate was placed 2cm to the right of the slit opening, forcing the mice to reach with their left paw. The female experimenter was blinded regarding mouse genotype during the test. The behavior was recorded from the front using a high-speed camera (Panasonic high-speed camera, HC-V750) at 1920×1080 px fixed at 50 FPS.

To clarify the session structure: sessions 1–5 were performed with pellet delivery using a spoon, whereas from session 6 onward pellets were presented on a plate positioned at the slot. During sessions 1–5, pellet placement was progressively adjusted to increase task difficulty (i.e., gradually positioned closer to the plate slot), thereby shaping forelimb reaching behavior. In session 6, the pellet was placed directly on the plate slot, requiring the animal to adapt its previously acquired reaching strategy.

Session terminology was defined as follows. Session 1 (“naive”) refers to the first spoon session and represents the animal’s first exposure to the forelimb reaching requirement; during prior habituation, mice retrieved pellets with the tongue and had not performed the reaching movement. Session 2 (“learning”) refers to the second spoon session, when animals already had initial task experience. This designation is supported by evidence that the majority of dendritic spines associated with motor learning are formed after the first training session [34], indicating that early structural plasticity is most prominent at this stage. Session 5 (“training”) refers to the final spoon session with facilitated delivery before the task configuration was altered. Session 6 (“retraining”) denotes the first session in which pellets were presented on the plate rather than the spoon, introducing a more challenging configuration that required behavioral adaptation.

For the caspase3 induced apoptosis group, after completing handling and habituation, 10 mice (4 $\text{Chrna2-Cre}^{\text{tg/wt}}\text{-tdTomato}^{\text{lx/wt}}$ and 6 $\text{Chrna2-Cre}^{\text{wt/wt}}\text{-tdTomato}^{\text{lx/wt}}$) were trained to take pellets from a spoon through the slit during four sessions, then trained to take pellets from the fixed position on the plate during three sessions. One mouse did not reach for pellets on the seventh session, and was therefore excluded. 9 mice (3 $\text{Chrna2-Cre}^{\text{tg/wt}}\text{-tdTomato}^{\text{lx/wt}}$ and 6 $\text{Chrna2-Cre}^{\text{wt/wt}}\text{-tdTomato}^{\text{lx/wt}}$) were selected and received viral vector injections (AAV5-FLEX-TACASP3-TEVP), followed by five more test sessions, starting at four weeks post-injection.

For the LFP group, 11 mice (5 $\text{Chrna2-Cre}^{\text{tg/wt}}$; 6 $\text{Chrna2-Cre}^{\text{wt/wt}}$) were used. After completing handling and habituation, the mice were trained during four sessions (session 1-4) to take pellets from a spoon through the slit, then trained for three sessions (session 5-7) to take pellets from the fixed plate through the slit. One mouse that did not reach for pellets in the seventh session was excluded. 13 mice (6 $\text{Chrna2-Cre}^{\text{tg/wt}}$ and 7 $\text{Chrna2-Cre}^{\text{wt/wt}}$) were selected and received viral vector injections (AAV9-hSyn-DIO-hM3Dq-mCherry), followed by six test sessions (session 8-13) with the headstage connected for LFP recordings four weeks post injections. The LFP signal was recorded with a 16-channel Intan RHD 2132 headstage connected to an Intan RHD2132 amplifier board by a thin flexible wire. Mice were briefly anesthetized with isoflurane in order to connect the headstage, then allowed to fully recover and placed inside the arena. Afterwards, mice were disconnected from the headstage and returned to their homecage. In the first three sessions after

viral injections (session 8-10) the mice received 0.9 % NaCl i.p. 45 minutes before the start of the recording. In the last three sessions (session 11-13) the mice received 0.01 mg/kg CLZ i.p. 45 minutes before the start of the recording.

For the group with repetitive Ma2 cell activation during learning, 14 mice (6 *Chrna2-Cre^{tg/wt}*; 8 *Chrna2-Cre^{wt/wt}*) were injected with viral vectors (AAV9-hSyn-DIO-hM3Dq-mCherry). Three to four weeks after viral injection, the handling and habituation was started. 45 minutes before the start of each session, the mice were injected with 0.01 mg/kg CLZ i.p. The first five sessions, the mice reached through the slit for pellets placed on a spoon. After five minutes in the fifth session, the pellet was instead placed on a fixed position on the plate, and the mice were encouraged to reach for it for five more minutes. The following five sessions, the mice reached for the pellet in the fixed position on the plate during ten minute long sessions. Mice with no reaches in more than three sessions were excluded from the analysis, which resulted in exclusion of one *Chrna2-Cre^{tg/wt}* mouse and three *Chrna2-Cre^{wt/wt}* mice. Three *Chrna2-Cre^{tg/wt}* mice were excluded due to no DREADD expression on post hoc tissue analysis.

For the miniscope group, 8 mice (5 *Chrna2-Cre^{tg/wt}*; 3 *Chrna2-Cre^{wt/wt}*) underwent viral injections and lens implant. 2 *Chrna2-Cre^{tg/wt}* did not have any detectable expression of the calcium indicator GFP Calmodulin M13 peptide 6 fast (GCaMP6f; checked with the miniscope under anesthesia before baseplate fixation), so they were excluded before the baseplate fixation step. The handling was started two to five weeks after lens implantation, followed by one additional habituation step in which the mice were habituated to the miniscope. The mice were then sedated with 1-4% isoflurane for two to five minutes while the miniscope was mounted on the baseplate and thereafter placed in a circular arena (diameter 45 cm) for 45 minutes, then returned to their homecage for 45 minutes and then once again placed in the circular arena for 45 minutes. After this habituation step the mice were sedated with 1-4% isoflurane for two to five minutes while the miniscope was disconnected from the baseplate. The mice were then returned to their homecage. A few days later, the mice underwent habituation to the single pellet prehension task as previously described, followed by six test sessions. 45-60 minutes before each test session the mice received 0.01 mg/kg CLZ i.p.. The miniscope was mounted on the baseplate on session 1, 2, 5 and 6. Only on those sessions, approximately 20 minutes after CLZ administration, the mice were sedated with 1-4% isoflurane for two to five minutes while the miniscope was mounted on the baseplate. After 20 minutes recovery from the sedation, the mice were placed in the prehension arena for ten minutes. In the arena, the cellular activity was recorded with the miniscope on session 1 (naive), 2 (learning), 5 (training) and 6 (pellet placed on the fixed plate; retraining) and the behavioral activity was recorded with the video camera on session 1-6. A blinking LED light was used to synchronize the time stamps of the miniscope recordings with the behavioral videos. After the test, the mice were sedated with isoflurane in order to remove the miniscope from the baseplate. Session 1-5 were performed every other day, session 6 was performed on the same day as session 5 directly after session 5. Data was recorded using a data acquisition device (DAQ) and a computer with Miniscope controller software installed. Focus of the miniscope was adjusted manually (300 μ m range). Optimal laser power (around 30% of max brightness), imaging gain, and focal distance was selected for each mouse and conserved across all sessions. The calcium signal was acquired at a frame rate of \approx 20 frames per seconds, with the timestamp of each frame registered onto a separate file.

Pasta Handling Test

The mice were tested in the pasta handling task, a quantitative assessment of skilled forelimb function, in order to measure forepaw dexterity [adapted from 30]. Mice were exposed to the pasta pieces (uncooked capellini pasta, 1.0 mm diameter, 2.6 cm length) in their home cage for five days to avoid neophobic reactions. Thereafter, the mice were habituated to eat inside the test arena (22 cm x 9 cm x 20.5 cm) for three days, without food restriction. After the habituation period, the mice were tested in the pasta handling test. The test consisted of sequential trials in which one pasta piece was delivered on the floor, in the center of the arena, for each trial. The behavior was recorded from the front using a high-speed camera (Panasonic high-speed camera,

HC-V750) at 1920×1080 px fixed at 50 FPS. Test sessions were performed after 15-20 hours of food restriction, starting at 5 p.m. the previous day. Each session of ten minutes consisted of a maximum of five trials. To make it easier to see how the capellini strand would move while being consumed, each pasta piece received a food coloring mark on one half. The number of pasta drops and the time spent handling the pasta was then quantified by visual inspection. 9 mice (3 *Chrna2-Cre^{tg/wt}-tdTomato^{lx/wt}*; 6 *Chrna2-Cre^{wt/wt}-tdTomato^{lx/wt}*) bilaterally injected with AAV5-FLEX-TACASP3-TEVP were tested in the pasta handling task six weeks after viral injection and one week after the last pellet prehension task session.

Hanging Wire Test

The coordination and strength of the forepaws was tested by the hanging wire test, in which mice suspend their body by holding on to a single wire stretched between two posts 40 cm above the ground. The mice were placed on the middle of the wire hanging from its forepaws for three minutes. A paper bed was placed between the two posts to avoid injury when the mice fell. The time hanging on the wire and number of falls were quantified by visual inspection. 9 mice (3 *Chrna2-Cre^{tg/wt}-tdTomato^{lx/wt}*; 6 *Chrna2-Cre^{wt/wt}-tdTomato^{lx/wt}*) were used. Mice were injected with viral vectors (AAV5-FLEX-TACASP3-TEVP) bilaterally, then performed the single pellet prehension task, and after completion of the single pellet prehension task, they performed the pasta handling and finally the hanging wire test (six weeks after the viral vector injection).

hM3Dq activation validation

Six weeks after the injection of AAV9-hSyn-DIO-hM3Dq-mCherry (n = 9 *Chrna2-Cre⁺* and 5 controls), CLZ 0.01 mg/kg was administered i.p. 135 minutes before transcardial perfusion and tissue preparation. After the administration of CLZ, before the transcardial perfusion, the mice were kept in their homecage. The mice were then deeply anesthetized with Medetomidin 1mg/kg (Dormitor Vet, Orion Pharma Animal Health) and Ketamin (Ketalar, Pfizer) 75 mg/kg i.p., before they were transcardially perfused as described below. After dissection and sectioning, immunohistochemistry for c-Fos and mCherry was performed as described below.

Tissue preparation and immunohistochemistry

To fix the tissue for post-hoc analysis, mice were anesthetized with Medetomidin 1mg/kg (Dormitor Vet, Orion Pharma Animal Health) and Ketamin (Ketalar, Pfizer) 75 mg/kg i.p. and sacrificed by transcardial perfusion with phosphate buffered saline (PBS, Fisher BioReagents, CAT 10051163) followed by 4% formaldehyde (VWR Chemicals BDH[®], CAT 9713.1000). The brains were dissected out and post-fixed in 4% formaldehyde overnight at 4°C, washed three times for ten minutes in PBS and then kept in PBS at 4°C until sectioning (a few hours or days). Before they were sectioned, the brains were embedded in 4% agarose in PBS. Sections were cut at a thickness of 70 μm using a Vibratome (Leica VT1000S) and then mounted with ProLong[™] Gold Antifade Mountant (ThermoFisher Scientific, CAT P10144) or Fluoroshield (Abcam) on glass slides (Superfrost[®] Plus, Thermo Scientific).

For the mice used in the hM3Dq activation validation, immunohistochemistry was performed. After sectioning these brains, the sections were washed in PBS and pre-blocked for one hour in 2% donkey serum (Biowest), 1% Bovine Serum Albumin (BSA, Sigma Aldrich), 0.1 % Triton[®]X-100 (Sigma Aldrich) and 0.05% Tween[®]20 (Sigma Aldrich) in PBS. The primary antibody, c-Fos(4)-G (goat polyclonal IgG, Santa Cruz Biotechnology, CAT K1314) or c-Fos (9F6) (Cell signaling, rabbit, #2250) and anti-mCherry (ThermoFisherScientific, 16D7, rat, M11217) were diluted 1:500 in 0.25% gelatin and 0.5 % Triton[®]X-100 in Tris-HCl buffered saline (TBS; 0.3% Tris, 0.8% NaCl and 0.02% KCl in mgH₂O, pH 7.4) and added to the sections. After 48 hours of incubation at 4°C the sections were washed with TBS and the secondary antibodies, donkey anti-goat A647 (ThermoFisherScientific A21447), donkey anti-rabbit A647 (ThermoFisherScientific A31573) and donkey anti-rat A488 (ThermoFisher-Scientific A21208) were diluted 1:500 in 0.25% gelatin and 0.5

% Triton[®]X-100 in TBS, added to the sections and incubated for 90 minutes at room temperature. The sections were washed with 0.1% Tween in TBS and distilled water before they were mounted on glass slides.

Imaging and image post processing

Most wide field images were acquired on a Zeiss Axio Imager Z2 (Zeiss, Germany) with a 10x objective (effective NA 0.45), a colibri LED 7 and Zen blue software (Zeiss, Germany), using a multi-band bandpass filter (Zeiss, Germany) with the filter excitation wavelengths 370-400 nm, 450-488 nm, 540-570 nm, 614-647 nm, 720-750 nm and the filter emission wavelengths 412-438 nm, 501-527 nm, 582-601 nm, 662-700 nm, 770-800 nm for the fluorophores DAPI, Alexa 647 and GFP and a single-band bandpass filter (TxRed-4040C-ZHE-ZERO, Semrock) with the excitation wavelengths 540-552 nm and emission wavelengths 590-4095 nm for mCherry. The light source used for the different fluorophores was LED-module 385nm for DAPI, LED-module 630 nm for Alexa 647, LED-module 475 nm for GFP and LED-module 567 nm for mCherry. Some images were taken using an Olympus BX61WI fluorescence microscope (Olympus, Japan) with a 10x (effective NA 0.40) objective and a Volocity 4.1.0 software (Quorum Technologies) or a Zeiss LSM700 confocal microscope (BioVis facility, Uppsala University). Brightness and contrast were adjusted in the Fiji software [35], equally for the whole image and without obscuring any data.

Pellet prehension task analysis

For each pellet prehension task session, the positions of the pellet, both forepaws, thumb, index and middle fingers were tracked. The AI network used for tracking (see Software availability) was trained specifically for detection of the left paw and the three fingers at the prehension onset position (paw palm pointing inside, thumb pointing up and fingers pointing to the medial line), and a tracking likelihood threshold of 70% was achieved from prehension onset to grasp end. Therefore, prehensions were reliably detected as blocks where the tracking likelihood for the left paw and its three fingers was above 70%. Prehensions were classified as successful when the animal reached for the pellet, grasped the pellet and brought it to its mouth. Any other outcome (mice hitting the pellet but failing to grasp it; missing the pellet; grasping the pellet but dropping it before it reached the mouth; reaching for the pellet when no pellet was available) was considered a failed prehension.

LFP electrophysiology analysis

Square voltage pulses were used to trigger LFP and miniscope recordings; and to drive a red LED placed at the top right corner of the behavioral camera field of view. Therefore, behavioral video recordings were synchronized with the corresponding electrophysiological recording by detecting the LED onset in the video. LFP data for each channel was filtered using a second-order Butterworth bandpass filter across the entire frequency range of 1-100 Hz, as well as within specific bands: theta (4-12 Hz), gamma (30-90 Hz), low theta (4-7 Hz), high theta (8-12 Hz), low gamma (30-40 Hz), and high gamma (60-90 Hz). This process was followed by the computation of the spectrogram, which offers a time-resolved representation of the frequency content in the data. The resulting spectrogram was normalized by dividing each power value by the cumulative mean, ensuring that the data reflected relative power rather than absolute magnitudes. Subsequently, average power values were extracted within the designated frequency bands by averaging over the frequency dimension, focusing specifically on the frequency bins that fell within the defined limits of each band.

In-vivo calcium imaging analysis

Neural signal extraction

The calcium signal in PCs was obtained using the viral vector with CamKII promoter driven expression of GCaMP6f. The increase in calcium levels corresponds to increased cell activity, and single spikes can only be indirectly estimated [36, 37, 38]. Miniscope videos were spatially downsampled 3x and motion-corrected, then cells signal was extracted using constrained

nonnegative matrix factorization for microendoscopic data (CNMF-E) approach [39], and fluorescence traces were detrended by baseline subtraction. The baseline components were estimated using a running 8th percentile derived from kernel density estimation over a 250-frame window, and subtracted from each respective trace. Although true F0 estimation is not possible on 1-photon data, the baseline-subtracted trace is here referred to as $\Delta F/F$. Neuron identity was matched along multiple recordings through intersection over union metric and the Hungarian algorithm for optimal matching. Up to this step, all miniscope video analysis was done as implemented previously [40].

Neural activity around prehensions

Prehension onset (time = 0 ms in all plots) was defined as the moment when the mouse's paw forms the grasp position, flipping the palm inside, thumb pointing up and fingers pointing to the medial line, then neurons fluorescence traces were sliced 1 s before and 1 s after forepaw prehension onset, and slices were grouped by prehension accuracy (successful or failed) and averaged separately for each session. To specifically assess how *Ma2* cell activity modulates pyramidal cell (PC) dynamics during prehension, we restricted our analyses to PCs that showed significant task-related modulation. For each neuron, we verified whether calcium activity is different between the before onset and after onset phases (ANOVA or Kruskal-Wallis, according to normality of distribution, evaluated using Shapiro's test). Only neurons that displayed a significant change in activity between these epochs were included in subsequent population, temporal, and assembly analyses. This approach ensured that our dataset was enriched for neurons that participate in prehension-related processing, rather than including large numbers of non-task-related cells that would dilute movement-specific effects. Using this criterion, 15.97% of recorded PCs were excluded because they did not show significant prehension-related modulation.

Pyramidal cell amplitude was calculated as the mean fluorescence of the averaged prehension window slices. For L5 pyramidal cells fluorescence peak latency analysis, traces for successful or failed grasps were separately averaged and normalized for each neuron, and neurons were sorted according to peak latency at successful grasps from each session. For PC response peak width, the width in seconds of the maximum response peak was calculated at half the peak prominence.

Assembly analysis

Additional constraints were required to allow for detection of assemblies between sessions. This limited the analysis to the naive, learning and retraining sessions, and only PCs detected through those sessions whose identity could be matched along sessions were kept. Therefore, on average 84.8 ± 14.2 PCs ($n = 4$ mice; 2 ctrl, 133 and 68; 2 *Chrna2-Cre+*, 77 and 61) were kept. Assemblies were identified during the entire 10 minute recording of a session, such that assembly detection was not affected by prehension accuracy. Assemblies were detected using independent component analysis with circular shifts [ICA-CS; 41], as implemented previously [42]. After removing neurons with no significant change comparing the before onset and after onset phases, only assemblies with 4 or more neurons and only neurons belonging to at least one assembly were kept for further assembly analysis. For calculating assembly spatial distribution, neurons from the assembly were first sorted according to their cartesian angle relative to the center of the assembly, which is the average of neurons' (x,y) coordinates. Finally, the assembly distribution was calculated as the area of the polygon formed by the sorted neurons. Assemblies resilience was calculated by finding the assembly with highest neuronal composition intersection on the other sessions according to the following formula:

$$\frac{\text{Size}(\text{Intersect}_{\text{Assembly1}-\text{Assembly2}})}{\text{Size}(\text{Assembly1})} + \frac{\text{Size}(\text{Intersect}_{\text{Assembly1}-\text{Assembly2}})}{\text{Size}(\text{Assembly2})} * \left(\left(\frac{\text{Size}(\text{Assembly2})}{\text{Size}(\text{Assembly1})} \right) - 1 \right) \quad (1)$$

such that resilience is within 0 (no intersection between assemblies) and 1 (exactly the same neurons forming both assemblies). To find assembly activity peaks, 1000 shuffles of activity of all neurons within an assembly on the time dimension were done, and activity peaks were considered as time samples where the sum of all neurons' real activity is larger than 95% of the sum of the shuffled neuronal activity, resulting in a rasterized activity (containing only 0 or 1 meaning inactive or active for each time point). Event histograms were calculated by slicing the assembly activity peaks in time windows of 2 s around each prehension (1 s before and 1 s after onset), where each bin corresponds to a one time sample of 50 ms, limited by the miniscope's 20 FPS recording speed. Assembly salience, a measurement of how relevant the activation (or silencing) of an assembly is within the prehension movement, was calculated as

$$\frac{\text{ActivityPeaksInWindow}}{\text{TimeSamplesInWindow}} - \frac{\text{ActivityPeaksOutWindow}}{\text{TimeSamplesOutWindow}} \quad (2)$$

such that salience is within -100 (assembly is active every time sample out of the prehension window and not active on any time sample within the window, i.e., absent prehension-related activity and full activity outside the prehension window) to 100 (assembly active in all time samples within the prehension window and at no time sample outside the window, i.e., full prehension-related activity and absent activity outside the prehension window).

Trial adjacency interference

To address whether closely spaced prehension attempts influenced baseline neural signals, we evaluated whether trials with inter-trial intervals ≤ 2 s (the full prehension window duration) showed significantly different calcium activity between "previous" and "current" trials. We determined if neural responses were significantly modulated by prior trials within this window using ANOVA or ANOVA-type statistics [43], based on normality testing via Shapiro's test. False discovery rate (FDR) correction was applied to p-values derived across all trial pairs using the Benjamini-Yekutieli procedure.

To further evaluate whether trial interference affects baseline neural signals, we analyzed fluorescence traces from time windows (-5 to -3 s) and (-3 to -1 s) relative to prehension onset, including only trials not preceded by another trial for at least 6 s. Fluorescence traces were sliced 5 s prior to 1 s prior to prehension onset, and grouped by genotype, training session and prehension accuracy (successful or failed) and averaged separately. An effect of time window epoch ((-5, -3) vs (-3, -1)) was determined via ANOVA or ANOVA-type statistics tests based on normality testing with Shapiro's test and used to identify baseline interference effects.

Statistical analysis

Differences were evaluated using mixed-models ANOVA, with post-hoc t-test for pairwise comparisons. Where the data showed non-normal distribution, evaluated using Shapiro's test, ANOVA-type statistics [43, mixed models] or Scheirer-Ray-Hare (independent factors) were used for multiple factors; Kruskal-Wallis with F-ratios [44] and ANOVA-type statistics tests were used for independent and dependent single factors, respectively; and post-hoc Mann-Whitney U or Wilcoxon signed-rank tests for independent and paired factors, respectively. All possible pairwise comparisons were computed, with multiple comparisons adjusted by Holm correction, and statistical significance conditioned to a false positive risk lower than $\alpha = 0.05$. In all figures, significance bars indicate significant comparisons ($p < 0.05$). The absence of these bars for any comparison means no significant difference was found ($p > 0.05$). Significance bars without ticks represent pairwise comparisons, while significance bars with downward ticks represent an effect. Error bars represent standard error of the mean (s.e.m) for all figures. For all violin plots, the filled area represents the entire data range, horizontal lines and triangle markers represent medians and means, respectively.

Software availability

LFP recordings were done using the Open-ephys GUI [45]. Calculations were done using Scipy [46], Numpy [47] and SciScripts [48], all plots were produced using Matplotlib [49] and schematics were drawn using Inkscape [50]. Cell fluorescence signals were extracted and processed from miniscope videos using CaImAn [40] and OpenCV [51]. Tracking of the mouse forepaw and fingers was done using DeepLabCut [52]. All scripts used for data analysis, including the DeepLabCut trained network, are available online [git repository; 53].

Results

Increased *Ma2* cell excitation affected calcium signal amplitudes in PCs during training and retraining

Considering the dual roles of the M1 as a motor control structure and a dynamic substrate that participates in motor learning [54], we were interested in how PCs were affected by modulation of *Ma2* cells during motor learning. For this purpose, we turned to chemogenetic manipulation using designer receptors exclusively activated by designer drugs [DREADDs; 55]. In pilot studies, we found that increased excitation of *Ma2* cells, but not increased inhibition, gave a measurable effect in a motor test (using modified Gq-coupled human M3 or Gicoupled human M4 muscarinic receptors [hM3Dq/hM4Di; 56]. We thus chose to continue with hM3Dq, and we first validated the effect of clozapine (CLZ) in *Chrna2-Cre+* mice. To validate the clozapine (CLZ) induced activation of hM3Dq+ cells, we injected viral vectors carrying the modified Gq-coupled human M3 muscarinic receptor (hDM3Gq) and the fluorescent marker mCherry [57] under Cre-dependent expression and performed immunolabeling for c-Fos, a proto-oncogene expressed in most neurons after depolarization [58, 59, Supplemental Figure 1A-B]. As expected, hDM3Gq activation induced c-Fos expression in *Chrna2-Cre+* mice (n=9; number of sections=346), on average, 32 mCherry-positive cells per hemisection were found, of which 76% were c-Fos positive. In control mice (n=5, number of sections=60), on average 5 mCherry positive cells per section were found, of which 0.8% were c-Fos positive (Supplemental Figure 1C). Throughout the manuscript, control mice refers to Cre-negative littermates that received the same treatment as the experimental *Chrna2-Cre+* mice. All calcium imaging recordings were performed with mice under clozapine 0.01mg/kg treatment.

Next, a prehension task, in which mice are encouraged to reach for and grasp a sugar pellet, was used to evaluate fine motor functions and motor skill learning [60, 61, 62]. Most dendritic spines that correlate with learning are formed after the initial training session and are maintained in the second training session [34]. Thus, we performed a set of recordings during the first “naive” session for collection of data in untrained mice, the second “learning” session and in the fifth “training” session to follow learning progression, and finally in a “retraining” session, during which a more challenging presentation of the pellet was introduced (Figure 1A-C). The contribution of increased *Ma2* cell excitation on individual PCs was investigated with calcium imaging. We recorded GCaMP6f fluorescence changes in cortical layer 5 using an implanted optical lens and prism assembled to a miniscope [Figure 1A; 63, 64]. To maximize the number of cells included in the analysis, PCs were separately identified for each session. Therefore, the number of PCs per animal varies for each session. On average, 61.4 ± 11.49 PCs (n = 6 mice; 3 Control, total of 1070 cells for 4 sessions, average of 105.2, 102.8 and 59.5 for each animal; 3 *Chrna2-Cre+*, total of 403 cells for 4 sessions, average of 45, 53.8 and 16) were included in the analysis. Calcium transients from individual cell activities were readily identifiable and showed diversified activity profiles (Figure 1D-E, Supplemental Figure 2A-H). Our analysis revealed no effect of genotype on prehension performance in a separate group of mice treated with CLZ before each session (n = 13 mice; 6 *Chrna2-Cre+* and 7 controls; Supplemental Table 1A-C; Figure 1F-H). However, mice learned the task (overall effect of training session for total number of prehensions, number of successful prehensions, and success ratio, Supplemental Table 1D-F), with an increase in the average number of total prehensions and successful prehensions from the naive to the training session, as well as an expected decrease in the retraining session due to increased difficulty. The

number of successful attempts per minute is an alternative measurement of learning progression, as the absolute number of attempts can increase disproportionately compared with the number of successful attempts, temporarily decreasing the success ratio even though the overall motor performance is still improving [61].

As expected, increasing *Ma2* cell excitation led to a decrease in baseline PC activity (non-prehension related) in *Chrna2-Cre+* mice compared to controls (Supplemental Figure 2I). When looking specifically at PC activity 2s around the prehension onset, our results showed an effect of session in PC amplitude on successful prehensions of controls (Supplemental Table 2A-C). PC activity amplitudes were decreased during successful prehensions in the learning session compared both to failed prehensions (Supplemental Table 2D) and to successful prehensions from the naive session (Supplemental Table 2E; Figure 1I-J). Furthermore, an overall effect of genotype on PC activity amplitude was found for the retraining session (Supplemental Table 2F), where PCs in *Chrna2-Cre+* mice exhibited an overall increased activity in the prehension window compared to PCs in control mice (Figure 1J).

We observed that a portion of prehensions overlapped with an already initiated prehension, within the time window of 2s. Specifically, in the naive session, 3.17% of successful and 36.07% of error prehensions occurred within 2s of a succeeding prehension. Similar proportions were found in later sessions: during learning (6.08% success, 28.26% error), during training (1.79% success, 28.12% error), and during retraining (4.76% success, 29.71% error). When considering all sessions combined, we found a total prehension overlap of 4.0% for successful and 29.91% for error prehensions. Perhaps this result is related to the fact that, when mice fail to get a pellet, they typically try again shortly, resulting in prehension overlaps. To address whether prehension-related neural activity affects baseline signals, we performed FDR-corrected trial-by-trial comparisons of adjacent trials, finding significant effect of the previous trial in the current trial in only 17.7% of pairs, indicating minimal influence of prior trials on calcium activity. Next, we selected trials not preceded by another trial for ≤ 6 s and compared the activity amplitude between the (-5, -3) and (-3, -1) time windows relative to prehension onset (Supplemental Figure 3A-H).

This analysis revealed no genotype- or session-related differences in baseline amplitude between epochs, though an interaction between accuracy and epoch emerged in the learning session (Supplemental Table 2G), driven by lower fluorescence in successful versus failed prehensions for control mice within the (-5, -3) window (Supplemental Table 2H; Supplemental Figure 3I). Collectively, these results confirm that prehension-related neural activity does not systematically alter non-prehension epochs.

We next aligned cell activity to prehension onset ($t = 0$), and measured the average PC population activity across two distinct phases: a one-second window before prehension (motor planning) and another one-second window during prehension (motor execution). We found similar effects (Supplemental Table 2I-J; Supplemental Figure 2J); reduced PC amplitudes for successful compared to failed prehensions from the learning session in control mice. Also, increased excitation of *Ma2* cells in the retraining session resulted in larger PC amplitudes when compared to controls (see summary Figure 6A). While baseline PC activity was decreased in *Chrna2-Cre+* mice, the amplitude of prehension-related PC activity was actually increased in these animals, particularly in the retraining session, which suggests a complex relationship between *Ma2* cell excitability and motor performance.

Finally, we investigated whether the activity proportion between planning and execution phases is affected by increased *Ma2* excitability, training, or prehension accuracy. We quantified the ratio of activity between the execution (during) and planning (before) epochs to assess how these factors modulate this proportion. We found a three-way interaction effect of genotype, session, and prehension accuracy (Supplemental Table 2K; Supplemental Figure 4), with genotype effects for both accuracies on the naive session and successful prehensions during the learning session (Supplemental Table 2L-N), and accuracy effects in control mice across the learning and training sessions (Supplemental Table 2O-P). This indicates that *Ma2* cell activity might selectively refine the neural signal balance during planning/execution phases of motor execution particularly on initial training sessions.

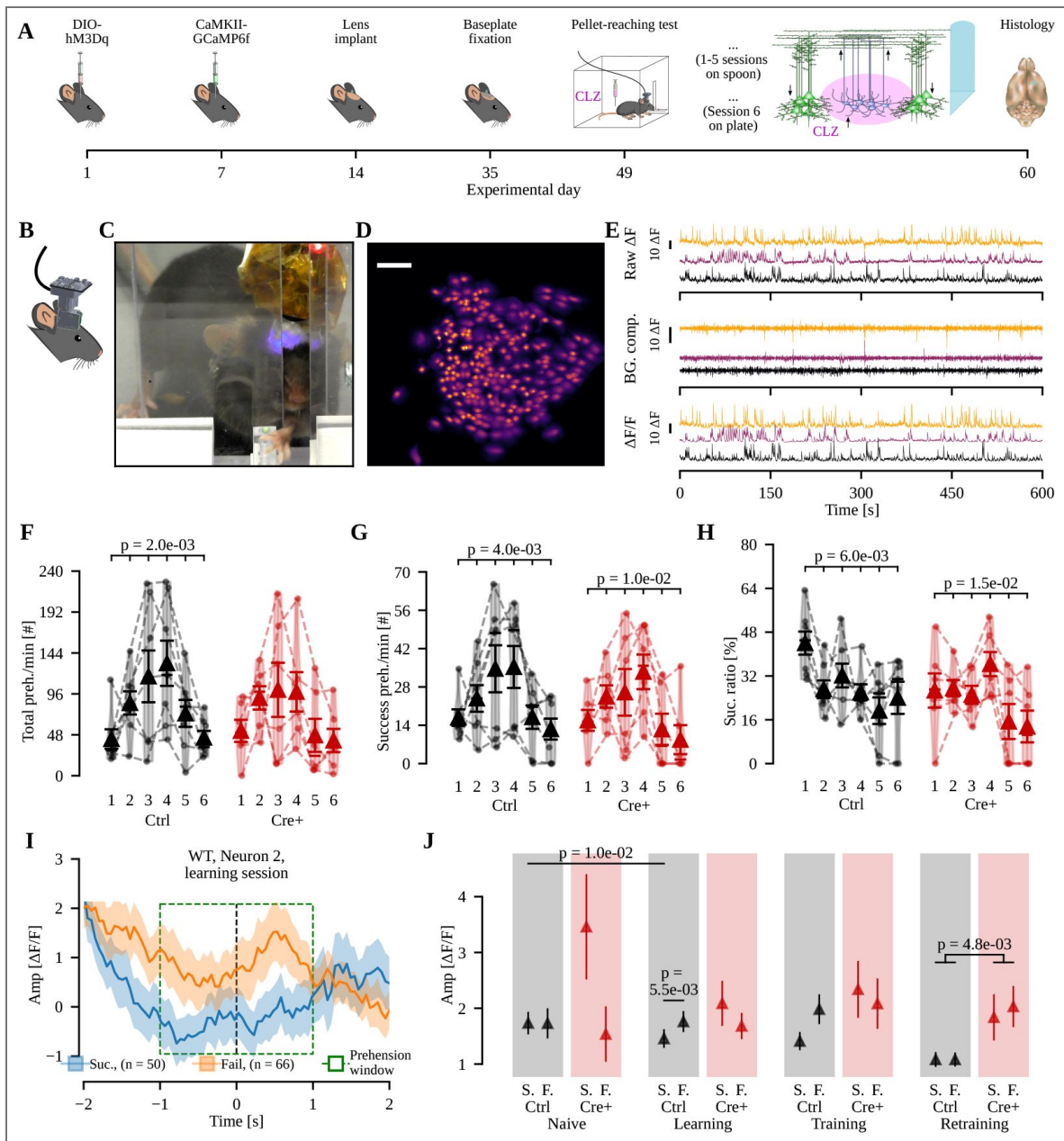


Figure 1. Mice with increased Ma2 cell excitability displays increased PC activity after training and upon retraining.

A) Timeline of experiments showing viral injections, miniscope lens implantation, base plate fixation and pellet-reaching task. GCaMP6f fluorescence and forepaw movements were recorded in naive, learning, trained and retrained sessions. B-C) Schematics (B) and photograph (C) of a mouse with the miniscope connected during prehension. D) Representative miniscope spatial footprints of L5 pyramidal cells after cell detection. Scalebar: 50 μm . E) Ten representative example fluorescence traces from PCs. F-H) Total number (F), success number (G) and success ratio of prehensions (H), separated by session and genotype (Controls, '-'; black; Chrna2-Cre+, '+', red). n mice = 7 Controls and 6 Chrna2-Cre+. I) Representative traces from a neuron of a control mouse showing the $\Delta\text{F}/\text{F}$ activity -2 to 2 second around the prehension onset, averaging all successful (Suc., blue) and failed prehensions (Fail., orange). J) Average amplitude of PC activity represented as mean \pm SEM, separated by session (naive, learning, training, retraining), genotype (Controls, '-'; black; Chrna2-Cre+, '+', red) and prehension accuracy (S., successful prehensions; F., failed prehensions). n cells per session = 162, 363, 399, 146 for Controls; 106, 126, 53, 118 for Chrna2-Cre+.

Increased *Ma2* cell excitation resulted in earlier PC firing during retraining

Changes in sequential activation of PCs are linked to learning [65]. Therefore, we next analyzed the temporal profiles of PCs, and identified the time point where they reached their maximum activity within the prehension window (Figure 2A-B). We compared the response peak latency between genotypes, sessions, and prehension accuracy while separating neurons based on the prehension phase where the activity peak is reached. For each session, the activity of each PC was averaged and normalized within the prehension window around prehension onset. We sorted individual neurons based on their latency to peak during successful prehensions and enforced the same sorting order for failed prehensions (Figure 2C). The peak latency analysis showed that PC temporal patterns were strongly affected by prehension accuracy (Supplemental Table 3A-C; Supplemental Figure 5; Figure 2D). This means that a large number of neurons changed their peak epoch in failed prehensions, such that neurons classified as “before neurons” in the successful prehensions can display peak latencies >0 in failed prehensions, while neurons classified as “during neurons” in successful prehensions can display peak latencies <0 in failed prehensions. In the failed prehensions from the learning session, PCs in *Chrna2-Cre+* mice had delayed responses compared to control mice (Supplemental Table 3D). In the successful prehension retraining session, PCs in *Chrna2-Cre+* mice displayed premature responses compared to PCs from control mice (Supplemental Table 3E). These premature responses occurred in the planning phase (before $t=0$). Together, these results suggest that temporal patterns shifted according to prehension accuracy, session and phase. Thus, increased *Ma2* cell excitation caused delayed PC firing during motor learning and premature PC firing on task retraining (Figure 6A).

We also measured the width of the response peak, a measure of the temporal specificity of cell activation that is proposed to influence motor accuracy [66, 67]. Broader response peaks indicate less temporal specificity. We analyzed the response peak width for each genotype across all training sessions, separating prehensions by accuracy (Figure 2E-H). The width of PC activity peaks was most strongly influenced by the session followed by genotype (Supplemental Table 4; Supplemental Figure 6; Figure 2I-J), where PCs in *Chrna2-Cre+* mice displayed overall sharper peaks compared to PCs in control mice, particularly during the training session (Figure 6A).

Increased *Ma2* cell excitation resulted in PC assembly salience rigidity, distribution compaction, and increased resilience

We next hypothesized that examination of PCs Hebbian assemblies could provide insights into how increased excitation of *Ma2* cells modulate cortical processing. In the assembly analysis, we focused on the naive, learning, and retraining sessions, retaining PCs detected through those sessions whose identity could be matched across sessions. On average, 84.8 ± 14.2 PCs were kept for the analysis. Prehension accuracy did not influence assembly identification, since we based it on neuronal activity across the 10-minute session recording, rather than only during the prehension window (Figure 3A). Assemblies consisting of less than four neurons, and neurons that were not part of any assembly, were omitted from the analysis. We identified a total of 23 assemblies in controls and 19 assemblies in *Chrna2-Cre+* mice, with an average number of 5.6 cells (SD 0.4) in each assembly for each session. The number of neurons within each assembly remained fairly consistent during learning and retraining (Figure 3B-E).

Motor training is associated with a selective increase in connectivity among task-related PCs [68]. On a PC population level, we examined assembly salience, here defined as the activity of the assembly within the prehension window in relation to its own activity outside the prehension window (ranging from -100 to 100; Figure 3F). The salience data for single assemblies varied from -2.04 to 24.62 and we found an overall effect of the training session on assembly salience (Supplemental Table 5A). Assembly activity during successful prehensions in control mice was less salient in the retraining session compared to the naive and learning sessions (Supplemental Table 5B-C; Figure 3G and 6B). We found no other differences in salience for failed prehensions or between training sessions in *Chrna2-Cre+* mice. This analysis suggests that the decreased activity

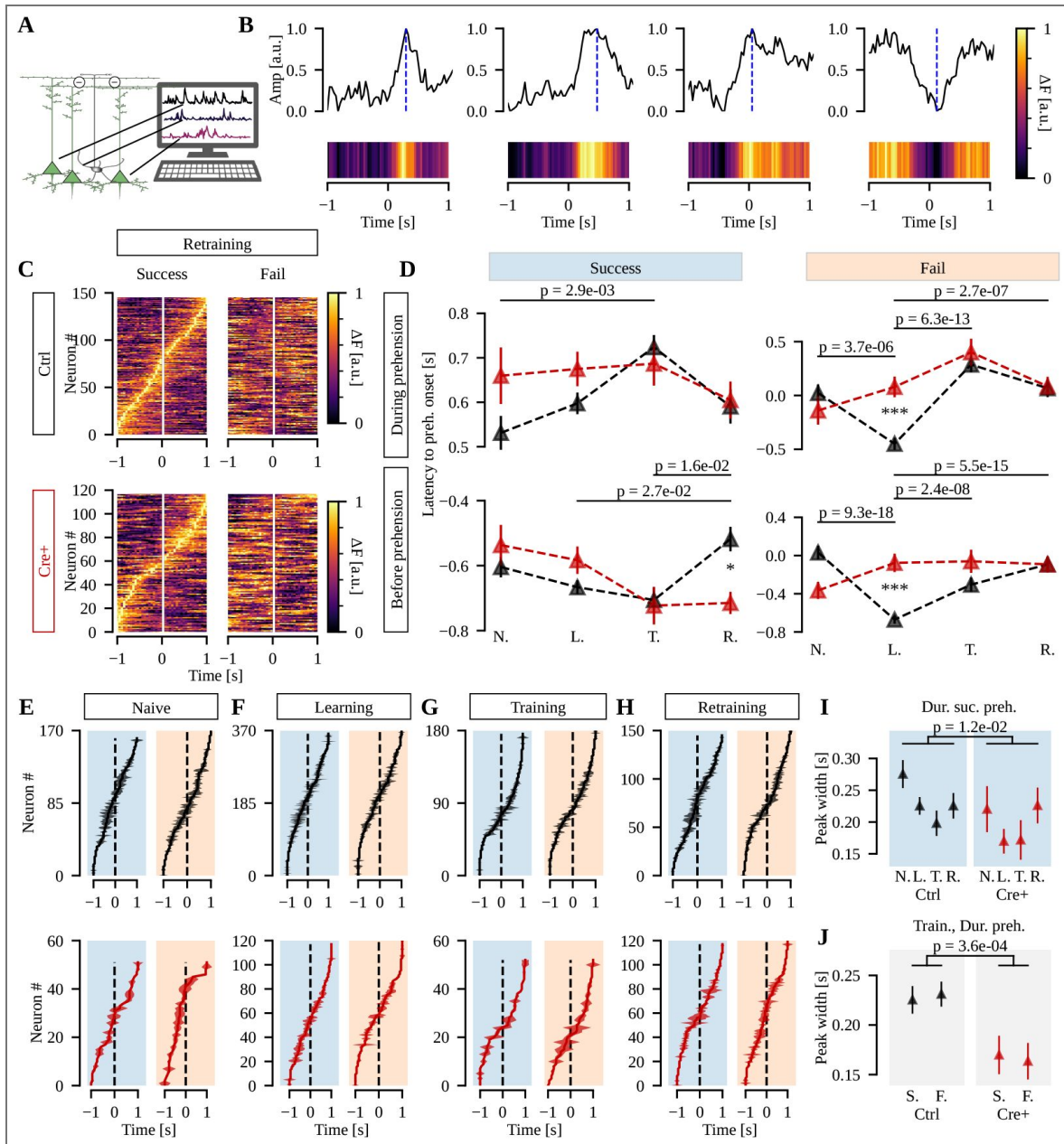


Figure 2. Increased excitation of Ma2 cells is associated with delayed PC activity during motor learning and premature PC activity on task retraining.

A) Illustration of recorded calcium signals from GCaMP6f-expressing PCs. B) Representative examples of average fluorescence traces around prehension onset for four different neurons, showing their normalized fluorescence curve ($\Delta F/F$ over time) represented in a colormap and latency of detected activity peaks (dashed blue line). C) Normalized average fluorescence matrices (Neuron \times Time \times F) for successful and failed prehensions, for control (top) and *Chrna2-Cre+* (bottom) mice, showing temporal activation patterns for each neuron on the retraining session. Neurons were sorted according to their temporal profile for successful prehensions, and follow the same order for failed prehensions. D) PC peak latency for both genotypes at each session before (bottom) or during (top) successful (left) and failed (right) prehensions. All significance bars refer to significant pairwise differences between sessions for controls; and asterisks represent significant pairwise differences between genotypes for a particular session. E-H) Peak latency with a shaded area indicating the peak width during naive, learning, trained, and retrained sessions for each neuron. At each plot, neurons were sorted according to their temporal profile. I-J) PCs response peak width during successful prehensions separated by genotype and session (I), and during prehensions from the training session separated by genotype and prehension accuracy (J). S., successful; F., failed; B., before; D., during prehension; N., naive; L., learning; T., training; R., retraining. n cells per session = 162, 363, 399, 146 for Controls; 106, 126, 53, 118 for *Chrna2-Cre+*.

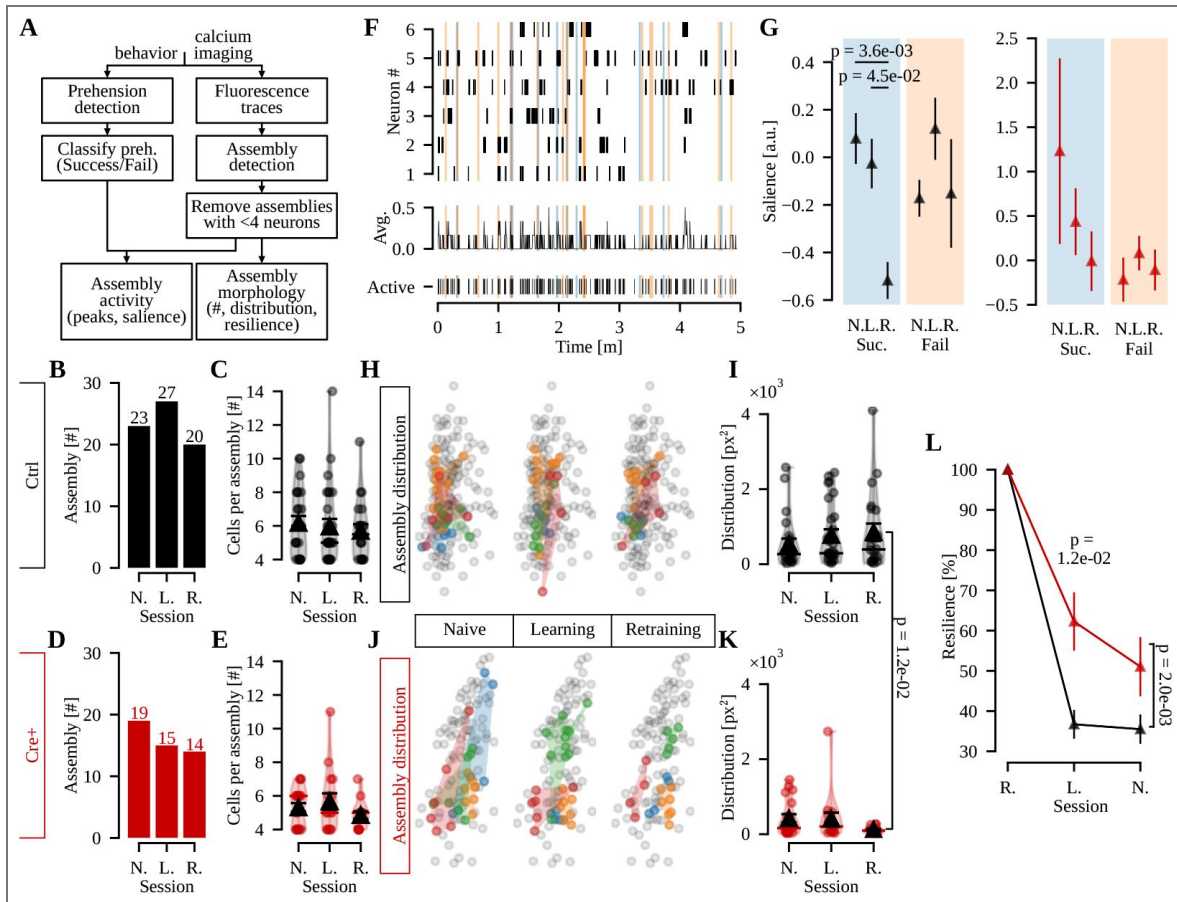


Figure 3. Mice with increased *Ma2* cell excitability display assemblies with less prehension-related activity, decreased spatial area and increased resilience.

A) Flowchart of the analysis pipeline. B-C) Number of assemblies and number of cells per assembly for control mice, detected at each session. D-E) Same as B-C, but for Cre+ animals. F) Activity of one representative assembly. Top, rasterized activity over the full recording time of the six neurons forming the assembly. Mid, the average of neuron activity. Bottom, the estimated rasterized activity of the assembly as a unit. Blue and orange shades show the successful and failed prehension windows, respectively. G) Saliency of assemblies during the whole 2s window for each session, grouped by genotype and prehension accuracy. H-I) Representative examples of 4 color-coded assemblies detected at session 6 and traced back to session 1 (H), and spatial distribution of detected assemblies at each session for control mice (I). J-K) Same as H-I, but for Cre+ animals. L) Resilience of assemblies for each genotype, for assemblies detected at retraining and followed back to the naive session. Suc., successful; Fail, failed; N, naive; L, learning; R, retraining.

observed in single neurons from control mice also occurs at the assembly level, where activity within the prehension window is decreased in relation to assembly activity outside the prehension window.

Functional imaging studies in humans show that brain activity varies regionally during different stages of motor learning [69]. Hence, we plotted the position of the individual PCs in each assembly and measured the spatial distribution which each assembly covered in the cortex. We found smaller assemblies in *Chrna2-Cre+* mice compared to control mice in the retraining session (Supplemental Table 5D-E; Figure 3H-K), suggesting that upon increased *Ma2* cell excitation assemblies were composed of PCs spatially closer together (Figure 6A-B).

To measure PC assembly plasticity, we investigated how much the assemblies had to change their neuronal composition to reach their final configuration in the retraining session, quantified here as assembly resilience. Resilience was calculated taking the assembly composition reported as the percentage of neuron match between sessions, with 100% being an assembly that did not incorporate or remove any neurons over time. We found that genotype and training session affected assembly resilience (Supplemental Table 5F), where assemblies in *Chrna2-Cre+* mice displayed increased resilience compared to assemblies in control mice in the learning session ($n = 20$ assemblies control and 14 assemblies *Chrna2-Cre+*; Supplemental Table 5G; Figure 3L). Together, these results suggest that PC assemblies undergo less modifications on their neuronal composition upon increased *Ma2* cell excitation (Figure 6A-B).

Increased *Ma2* cell excitation resulted in improved execution of a learned motor task

So far, we found that increased *Ma2* cell excitation resulted in several effects on PC population and assembly plasticity in the motor cortex (Figure 6A-B). Notably, despite these changes in neural activity, we found no effect of genotype on prehension performance (Figure 1F-H; Supplemental Table 1A-C), which highlights a potential dissociation between changes in neural activity and performance outcomes. Since we observed changes related to plasticity with no effect on learning outcome when activating *Ma2* cells repetitively, we instead wanted to evaluate the potential effect of *Ma2* cell activation on already acquired motor skills. To investigate the possible influence of increased *Ma2* cell excitability on already learned motor skills, we trained mice (*Chrna2-Cre+*, $n = 5$; control, $n = 6$) for seven sessions prior to injecting them with hM3Dq and then evaluated their performance in a prehension task (Supplemental Figure 7A). In the first three post-injection sessions (8, 9 and 10), saline was administered to assess potential injection effects, while CLZ was administered in the following three sessions (11, 12 and 13) to measure the potential impact (Figure 4A). We found an overall effect of session in the success rate (Supplemental Table 1G-H), and when grouping by genotype we found that CLZ treatment increased the success rate in *Chrna2-Cre+* mice compared to saline treatment, which was not observed in control mice (Supplemental Table 1I-L; Figure 4B). These results suggest that enhancing *Ma2* cell excitability improved the execution of an already learned fine motor task (Figure 6C).

Low and high sub-bands within theta and gamma frequencies are associated with different functional roles in attentional control, sensory integration, and fine motor control. To gain deeper insight into how *Ma2* cell modulation affects motor planning and execution, we recorded local field potentials (LFPs) in the same mice during task performance in the CLZ-treated sessions (sessions 11–13). This allowed us to correlate neural activity patterns with specific phases of the task. We separated successful and failed prehensions and analyzed one-second time windows before (planning phase) and during (execution phase) task onset. Using spectrograms, we calculated power in various frequency bands across the LFP signal, spanning 1–100 Hz, with specific focus on the theta (4–12 Hz) and gamma (30–90 Hz) ranges. The theta band was further divided into low (4–7 Hz) and high (8–12 Hz) frequencies, and gamma was divided into low (30–40 Hz) and high (60–90 Hz) frequencies (Figure 4C).

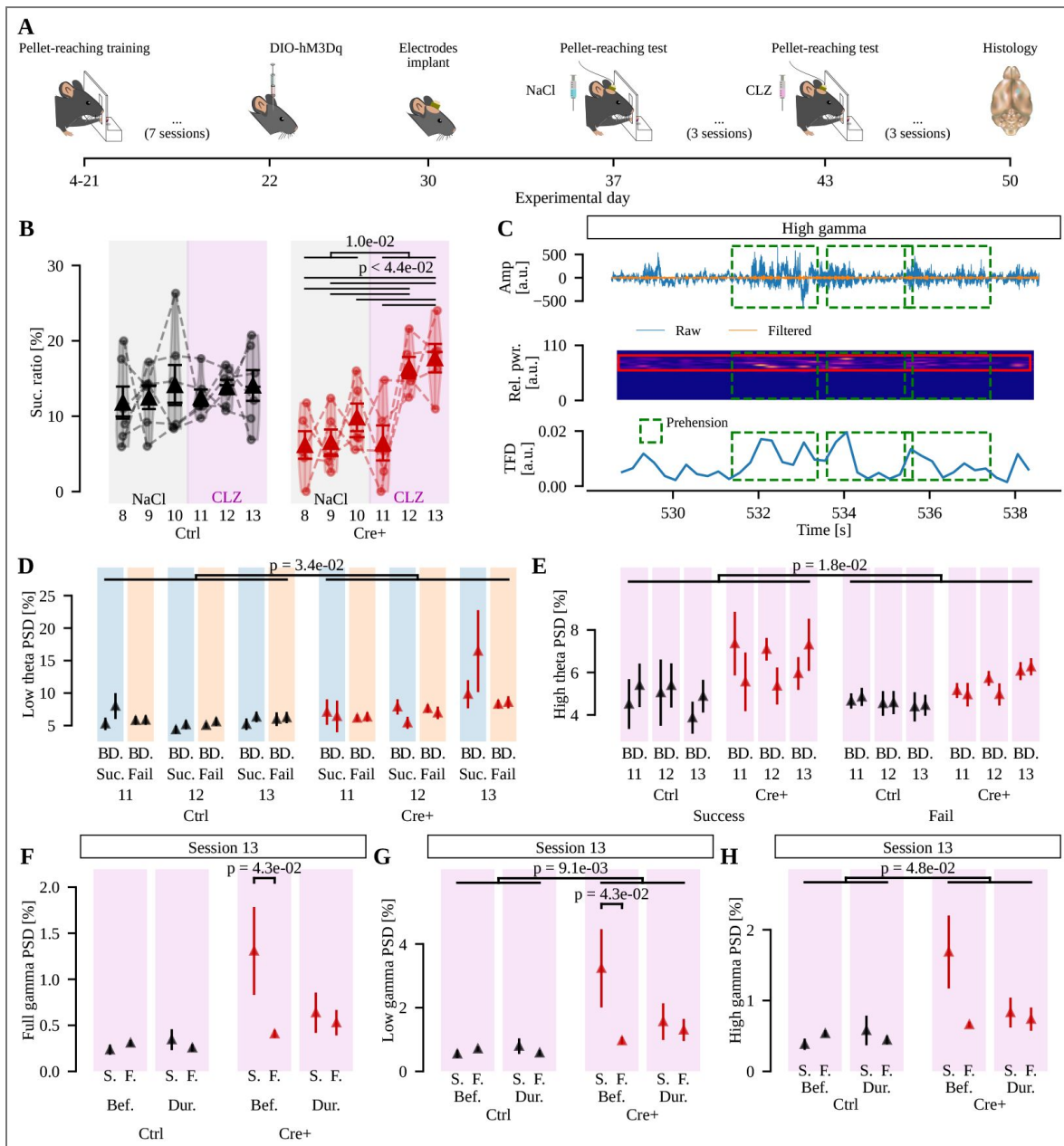


Figure 4. Mice with increased Ma2 cell excitability display increased prehension success rate, increased LFP low theta and gamma power.

A) Timeline of the experiments. Animals were trained to reach for the pellet and after the 7th session, the hM3Dq was injected and the LFP electrodes implanted. B) Prehension success ratio for control (Left, black) and Chrna2-Cre+ (Right, red) mice in the sessions with saline injection (gray shade) and clozapine injection (purple shade). C) Example of time-frequency domain power processing, with three prehensions highlighted (green dashed squares). Top, raw (blue) and high gamma-filtered (orange) LFP traces. Mid, spectrogram from the filtered signal, with highlights for the high gamma band (red square). Bottom, the time-frequency domain power over time, calculated as the average of the previously highlighted spectrogram region. D-H) Relative power for low theta, high theta, full gamma, low gamma and high gamma, respectively. D and E shows the full dataset due to the observed overall effects, while for F-H only isolated effects for session 13 were found. Shades: blue and orange (successful and failed prehensions); magenta (sessions under CZP treatment). Abbreviations: B. or Bef., before prehensions; D. or Dur., during prehensions; S. or Suc., successful prehensions; F. or Fail, failed prehensions. n mice = 6 Controls and 5 Chrna2-Cre+.

LFP analysis provided a detailed view of *Ma2* cell involvement, showing increased power in the full theta band and the low theta band in *Chrna2-Cre+* mice compared to controls (Supplemental Table 6A-C; Figure 4D [↗](#)). Notably, in the high theta band, we observed higher power in successful than failed prehensions (Supplemental Table 6D; Figure 4E [↗](#)). Session 13 showed similar trends, with higher power in successful than failed prehensions across gamma bands (Supplemental Table 6E-F; Figure 4F-H [↗](#)). For the low gamma band, *Chrna2-Cre+* mice displayed higher power than controls, especially in successful prehensions (Supplemental Table 6G-H; Figure 4G [↗](#)). High gamma power was also elevated in *Chrna2-Cre+* mice compared to controls (Supplemental Table 6I-J; Figure 4H [↗](#)).

We next evaluated the LFP power outside prehension epochs, i.e., when no prehension movement was being performed. Analysis showed an interaction effect of genotype and session across all frequency bands (Supplemental Table 6K). For full, theta, and beta bands, these interactions were driven by a session effect in *Chrna2-Cre+* mice (Supplemental Table 6L, Supplemental Figure 7B-E), with LFP power in session 13 consistently decreased compared to previous sessions, not observed in control mice. When subdividing theta and gamma into low and high subdivisions, low-theta power was affected both by genotype and training session (Supplemental Table 6M-N, Supplemental Figure 7F). Similarly, genotype affected both low- and high-gamma bands (Supplemental Table 6O-P, Supplemental Figure 7G-H). No effects were found for the high-theta band.

Collectively, these findings suggest that *Ma2* cell activation plays a role in increasing low theta and gamma power during motor planning and execution phases of a learned task, while reducing overall LFP power when no prehension is being performed, supporting a role for *Ma2* cells in fine-tuning motor performance (Figure 6C [↗](#)).

Ablation of *Ma2* cells affected fine motor functions

To investigate how the absence of *Ma2* cells might affect motor execution, we used a Caspase-based virus approach to selectively ablate these cells in the forelimb area of the M1 of *Chrna2-Cre/tdTomato* mice. After unilateral injections ($n = 2$; Figure 5A [↗](#)), the deletion resulted in a reduction of 80.4% of the number of tdTomato-positive cells on the injected side compared to the uninjected side within the same mouse (Figure 5B [↗](#)). Initially, we used a pasta handling test to assess forepaw dexterity that does not require training and found that bilaterally injected *Chrna2-Cre+* mice dropped more pasta than control mice ($n = 3$ *Chrna2-Cre+*, 6 controls; Supplemental Table 1M), although their handling times were similar (Figure 5C-E [↗](#)). We also used a hanging wire test to evaluate grip strength and endurance [70], but found no differences between the two groups in terms of number of falls or time spent on the wire (Figure 5F-H [↗](#)). In the prehension task, we found an overall effect of training session in the success ratio (Supplemental Table 1N), but we did not find an effect of genotype in the prehension's success ratio (Supplemental Table 1O), only a punctual pairwise difference between sessions 7 and 10 (Figure 5I [↗](#), Supplemental Table 1P). Thus, ablation of *Ma2* cells did not affect prehension task success, but reduced dexterity in the pasta handling test. This suggests that *Ma2* cells may have a role in orchestrating precise forelimb movements that do not require previous specific training (Figure 6C [↗](#)). Together with results from the group where mice with increased excitability of *Ma2* cells displayed improved performance compared to baseline, these findings suggest that although *Ma2* cells may contribute to fine-tuning motor performance, they are not essential for executing learned complex movements.

Discussion

Here we investigated how *Ma2* cells impact PC population dynamics during motor learning and execution. We found that, upon increased *Ma2* cell excitation, parameters of plasticity at the cell, population and assembly level, all indicate decreased plasticity (Figure 6A-B [↗](#)). Whereas increased *Ma2* cell excitation during training did not affect prehension accuracy, it did improve

Figure 5. Apoptosis in Ma2 cells decreased pasta handling performance.

A) Timeline of the experiments. B) Unilateral injection of Cre-dependent TACASP3 decreased the amount of Chrna2-Cre+ cells in the motor cortex by 80.4%. Enlargement of the injected motor cortex (B'), and contralateral non-injected side (B''). Scalebars: 500µm (B) and 200µm (B' and B''). C) Animal performing the pasta handling task. D-E) Graph of results on pasta drops and time spent in the task. F) Animal performing the hanging wire task. G-H) Graph of results on falls and time spent in the task. n mice = 6 Controls and 3 Chrna2-Cre+. I) Single pellet prehension task before (session 7) and after ablation (sessions 8-12) for WT (black) and Chrna2-Cre+ mice (red). n mice = 8 Controls and 6 Chrna2-Cre+.

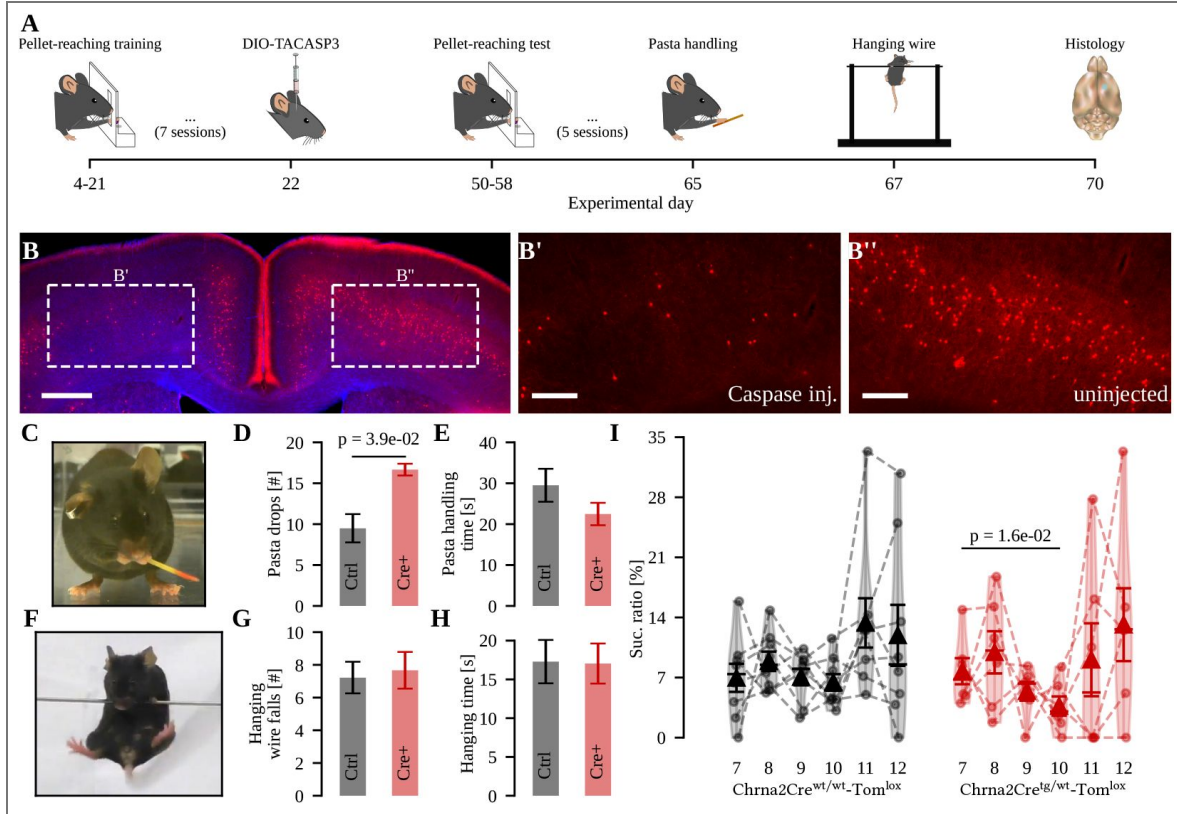
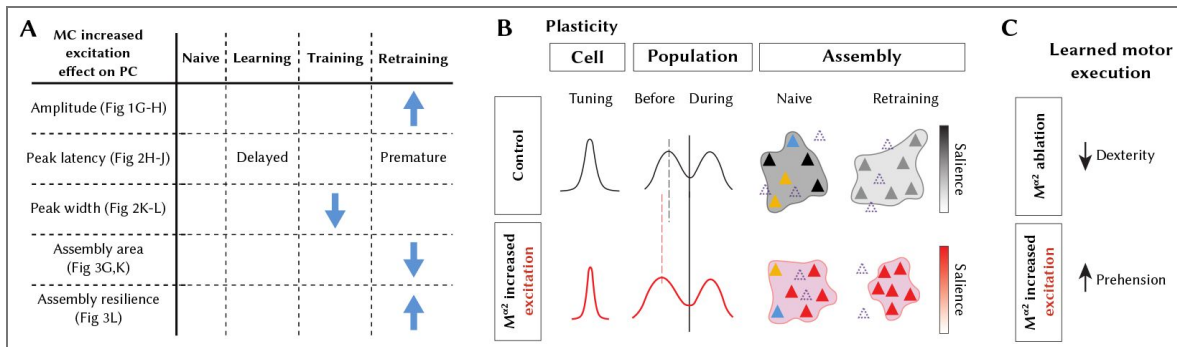


Figure 6. Summary of findings.

A) Table summarizing the effects of increased Ma2 cells excitation on PCs. B) Schematic outline illustrating plasticity parameters. Increased excitation of Ma2 cells resulted in more narrow tuning of layer 5 PCs, a temporal shift of the average population activity both in the motor planning and execution phases, enhanced resilience, reduced physical assembly coverage and rigid salience upon retraining. Dashed triangles mark PCs that are part of the retrained assembly but not the naive assembly, and vice versa. Blue and yellow depict PCs in the naive assembly that are part of another assembly in the retraining session. Salience values are represented by the degree of color in PCs and assembly distributions. C) Ma2 cells influence fine motor movements, where caspase induced ablation of Ma2 cells resulted in decreased dexterity, whereas increased excitation of Ma2 cells resulted in increased accuracy.



the success rate when chemogenetic activation was initiated in mice that had already learned a task (Figure 6C). Thus, our data suggest that increased *Ma2* cell excitation seems to reduce PC plasticity while possibly facilitating an already acquired motor skills.

Lateral inhibition, a canonical function of inhibitory circuits and Martinotti cells (MCs) in particular, sharpens excitatory responses and promotes competitive interactions among pyramidal cells [PCs; 71, 15]. By suppressing neighboring PCs, early activated cells can dominate network output, implementing a winner-take-all strategy in which temporally leading PCs emerge as influential “leader” cells. Consistent with this framework, motor learning shifts the temporal activation of L2/3 PCs toward earlier firing [11], and our calcium imaging data likewise show that temporal activation patterns, rather than response amplitudes, predict successful prehension. Successful trials were characterized by an early PC peak during the planning phase followed by a later peak during movement execution, underscoring the importance of precisely structured temporal dynamics.

Although SST interneurons have been shown to enable and maintain sequential PC activation during motor learning [11], accumulating transcriptomic and circuit-level evidence demonstrates that SST cells comprise multiple molecularly and functionally distinct subtypes [72, 21], which can display layer-specific and even opposing activity patterns [16]. Broad SST manipulations therefore likely engage heterogeneous populations with divergent functions. In contrast, we targeted a homogeneous layer 5 Martinotti subtype [*Ma2* cells; 24] and found that increasing *Ma2* excitability shifted PC peak activity toward the motor planning phase, enhanced directional tuning precision, and improved execution of an already learned movement without affecting acquisition. This contrasts with reports of impaired motor learning following global SST activation [73, 74] and supports the idea that distinct SST subpopulations differentially regulate learning and execution phases. Mechanistically, enhanced *Ma2* activity likely sharpens tuning [66, 67], promotes temporal synchronization of layer 5 PCs [24], and stabilizes assembly structure during retraining, thereby biasing the emergence of temporally leading “leader” PCs. Together, our findings support a model in which layer-specific SST subtypes sculpt PC temporal dynamics and assembly plasticity in a phase-dependent manner during motor behavior.

Importantly, our conclusion that *Ma2* activation dissociates neural dynamics from performance outcomes should be interpreted within the limits of our behavioral measurements. Motor performance was quantified primarily as prehension success rate. While this metric captures task outcome, it does not resolve finer kinematic parameters such as reach trajectory, movement speed, acceleration profiles, or grip force. It therefore remains possible that *Ma2* modulation affects additional aspects of motor execution that were not measured here. Future studies combining neural recordings with detailed kinematic analyses will be important to determine whether the observed changes in PC temporal dynamics are also reflected in subtler alterations of movement structure.

Temporal properties differ between interneuron populations, and similarly, PCs are likely to be variably inhibited depending on timing, synaptic weights, and the position of the interneuron contact [75]. Notably, a hypothesis postulates a central role of local inhibitory drive in tuning motor circuits for accuracy [66, 67]. A strong inhibitory drive would narrow directional tuning widths and lead to more accurate movements. Our experimental data on motor execution adhere to and support this theory, since we found that heightened excitation of *Ma2* cells, i.e. more inhibition, resulted in improved accuracy and narrower PC activity tuning (Figure 6C).

In addition to sharpening responses via lateral inhibition, *Ma2* cells can actively promote synchronization of pyramidal cell (PC) activity. Because each *Ma2* interneuron targets the distal dendrites of multiple PCs, their coordinated firing, or release from inhibition, can impose a shared inhibitory timing signal across a local PC population. This can align the timing of PC spikes and thereby promote synchronous firing. Indeed, in layer 5 neocortex, optogenetic activation of *Ma2* cells were shown to transform previously uncorrelated PCs into temporally synchronized ensembles, particularly among type A pyramidal cells [24]. Such synchronization depends critically on the firing pattern of the interneurons, underscoring that inhibition does not merely suppress activity but actively structures the temporal coordination of excitatory networks. In the

context of our data, this provides a mechanistic framework for how increased *Ma2* cell excitation could bias the emergence of “leader” PCs and constrain assembly reconfiguration during retraining by enforcing tighter temporal coupling among layer 5 PCs.

Hebbian learning postulates that when neurons fire synchronously, they reinforce synaptic efficiency and form an assembly. The original theory has been extended to include all cells with above-chance interactions, leading to variable definitions of neural assemblies [76]. We here adhere to the proposition that assemblies are formed by neurons that together increase their average firing rates for a specific period [77, 41], and that they can harbor varying degrees of temporal precision, scale and internal structure [78]. According to the extended theory, assemblies dynamically form, reconfigure, and fire simultaneously, with a reduced number of cells triggering the entire assembly [79]. The theory also proposes that one single neuron could participate in multiple neural assemblies, leading to distributed information coding. When PCs in our data set were sorted into assemblies, we found that the average number of cells composing the assemblies were similar regardless of *Ma2* cell activation state. Notably though, the distribution of each assembly, which remained constant during learning and retraining sessions in control mice, were smaller during retraining in mice with increased *Ma2* cell activity, demonstrating that *Ma2* cell activity can affect PC cell assembly internal structure. In learning and retraining sessions, increased *Ma2* cell excitation resulted in an increased resilience in PC assemblies, suggesting that increased *Ma2* cell excitation decreases PC assembly plasticity. Accordingly, during retraining, the assembly salience decreased in control mice, but not in *Chrna2-Cre+* mice, further supporting that increased *Ma2* cell excitation decreases plasticity and network reorganization (Figure 6A-B [80]).

In the motor cortex, different motor tasks induce dendritic calcium spikes on different apical branches of individual PCs, which reduces the chance of acquired skills to be disrupted by the formation of new motor programs. Intriguingly, after SST interneuron ablation, the maintenance of synaptic potentiation acquired during previously learned tasks is lost, resulting in decreased performance [3]. We found, after ablation of *Ma2* cells, an increased number of drops in the pasta handling task. Thus, *Ma2* cells, as part of the SST population, also seem important for facilitating execution and refining already acquired fine motor skills. Further, it has been shown that increased SST interneuron activity helps maintain previously acquired motor skills when executing a slightly different motor task, whereas decreased SST interneuron activity is important for improved motor performance and learning of the initial motor task [11, 80]. Also, the initial learning phase involves weak cortical activation of SST interneurons, and even though individual SST interneurons show diverse activity profiles during movement phases in a lever-press task, the average activity of SST interneurons increases as learning progresses [80]. We found that increased excitation of *Ma2* cells during execution of a learned motor task, the single-pellet prehension task, improved the success rate. However, in contrast to what has been shown for SST interneurons in layer 2/3 [11], repetitive increased excitation of *Ma2* cells during training did not affect motor performance. Hence, it seems that increased excitation of *Ma2* cells, resulting in decreased PC assembly reconfiguration and plasticity, mainly influences the execution of already acquired motor skills and that decreased motor learning during SST interneuron activation is likely mediated by other SST interneuron subpopulations. It has been suggested that layer specific network activity takes place during learning of a motor task, where the L2/3 network seem to represent coordination of signals during learning, whereas L5a may participate in networks for well-learned movements [81].

The network of inhibitory interneurons is essential for generating gamma rhythms [82]. Previous studies have highlighted the critical roles of parvalbumin and somatostatin interneurons in sustaining gamma activity in both the cortex and hippocampus [83, 84]. Research involving local field potentials (LFPs) in monkeys and humans has shown an increase in high gamma power (70–170 Hz) alongside a decrease in beta power (8–30 Hz) prior to and during forelimb movements [85, 86, 87]. In rats, high gamma power was also observed during upward movements in a reaching task, measured through epidural field potentials (EFPs) and LFPs [88], where both demonstrated an increase in high gamma power during upward reaches. Additionally, power increases in the high gamma band (70–170 Hz) were noted just before movement onset for upward, left, and right

reaches across different tasks [88]. Our results pinpoint a role for *Ma2* cells in gamma and theta oscillations during motor performance, particularly in the context of successful versus failed trials. The elevated high theta power in the success trials compared to failed trials, and increased power in low and high gamma oscillations in *Chrna2-Cre+* mice compared to controls, suggests that *Ma2* cells may be important for motor planning and execution. Overall, these findings reveal a complex interplay between *Ma2* activity, oscillatory brain dynamics, and motor function, prompting further investigation into how these mechanisms impact behavioral outcomes.

A limitation of our design is the absence of a *Chrna2-Cre+* group expressing a Cre-dependent control vector without hM3Dq. In principle, we therefore cannot fully exclude effects of viral expression per se. However, several observations argue against this interpretation. Cre-dependent expression alone has repeatedly been shown not to affect behavior or network activity in the absence of DREADD activation [89, 90, 91]. We also controlled for nonspecific clozapine effects by administering the same low dose to *Chrna2-Cre+* and control mice, and verified effective hM3Dq activation via c-Fos induction in *Ma2* cells. Finally, we observed no effect of Cre-dependent hM3Dq expression alone in our LFP controls (Figure 4). Together, these data make it highly unlikely that the reported effects are driven by viral expression rather than increased *Ma2* cell activity.

In conclusion, we have identified a role for *Ma2* cells in PC population dynamics, motor learning and execution. We find that activation of layer-5-specific Martinotti cells improves the execution of an already learned task, whereas learning efficiency of the task is unaffected, functionally separating these two aspects of motor activity. Even so, *Ma2* cells are involved in temporal shaping of PC population dynamics and impact several aspects of assembly plasticity during motor learning, training and retraining. Further studies are warranted to address the activity patterns of *Ma2* cells themselves during motor learning and execution, and also whether modulation of *Ma2* cell activity can affect other types of learning and skills emanating from other cortical areas.

Data availability

All data analyzed during this study are included in the manuscript and supporting files. All code used is openly accessible at <https://gitlab.com/malfatti/M1MartinottiOnMovement>.

Acknowledgements

We thank Uppsala University behavioral facility (UUBF) and Charité for support and reagents, Juan Jiang, UmU, for establishing the prehension task.

Additional information

Author Contributions

Methodology (AV, JW, BC, RL), Data curation (AV, JW, BC, KH), Validation (AV, JW, BC), Software (GN, TM), Formal analysis (TM, AV, KH, GN), Visualization (TM, BC, AV, KH, KK), Original draft preparation (KK, TM, AV, BC), Conceptualization (KK, AV, RL), Writing-Reviewing and Editing (KK, TM, BC, AV).

Funding

We thank the Swedish Foundation for International Cooperation in Research and Higher Education (STINT; www.stint.se), the Swedish Research Council (2018-02750, 2022-01245; www.vr.se) the Swedish Brain Foundation (FO2020-0228, FO2022-0018; <http://hjärnfonden.se>), Program for Institutional Internationalization (CAPES - PrInt, 88887.574901/2020-00), the Wenner-Gren foundations (UDP2020-0006) and Olle Engkvist Byggmästare Foundation (220-0254; <https://engkviststiftelserna.se>).

Funding

Funder	Grant reference number	Author
Swedish Foundation for International Cooperation in Research and Higher Education (STINT)		George Nascimento
Swedish Foundation for International Cooperation in Research and Higher Education (STINT)		Richardson N Leao
Swedish Foundation for International Cooperation in Research and Higher Education (STINT)		Jessica Winne
Swedish Research Council	2022-01245	Katharina Henriksson Klas Kullander Anna Velica
Swedish Brain Foundation	FO2022-0018	Katharina Henriksson Klas Kullander Anna Velica Thawann Malfatti
Coordenação de Aperfeiçoamento de Pessoal de Nível Superior (CAPES)	88887.574901/2020-00	Barbara Ciralli
Wenner-Gren Stiftelserna (Wenner-Gren Foundations)	UDP2020-0006	Thawann Malfatti
Olle Engkvists Stiftelse (Stiftelsen Olle Engkvist Byggmästare)	220-0254	Barbara Ciralli

Author ORCID iDs

Thawann Malfatti: <https://orcid.org/0000-0001-9672-9995>

Anna Velica: <https://orcid.org/0000-0002-4604-2949>

Jéssica Winne: <https://orcid.org/0000-0002-5167-1053>

Barbara Ciralli: <https://orcid.org/0000-0003-4021-2668>

Katharina Henriksson: <https://orcid.org/0000-0002-5158-1912>

George Nascimento: <https://orcid.org/0000-0002-6572-1269>

Richardson Leao: <https://orcid.org/0000-0001-8496-1965>

Klas Kullander: <https://orcid.org/0000-0001-6418-5460>

Additional files

[Supplemental material](#) 

References

- [1] Vargas-Irwin C. E., Shakhnarovich G., Yadollahpour P., Mislow J. M. K., Black M. J., Donoghue J. P. (2010) Decoding complete reach and grasp actions from local primary motor cortex populations. *Journal of Neuroscience* **30**:9659-9669 <https://doi.org/10.1523/jneurosci.5443-09.2010> | PubMed
- [2] Metz G.A.S, Dietz V., Schwab M.E., van de Meent H. (1998) The effects of unilateral pyramidal tract section on hindlimb motor performance in the rat. *Behavioural Brain Research* **96**:37-46 [https://doi.org/10.1016/s0166-4328\(97\)00195-2](https://doi.org/10.1016/s0166-4328(97)00195-2) | PubMed
- [3] Cichon Joseph, Gan Wen-Biao (2015) Branch-specific dendritic ca2+ spikes cause persistent synaptic plasticity. *Nature* **520**:180-185 <https://doi.org/10.1038/nature14251> | PubMed

- [4] Rioult-Pedotti Mengia-S, Friedman Daniel, Donoghue John P (2000) Learning-induced ltp in neocortex. *science* **290**:533-536 <https://doi.org/10.1126/science.290.5491.533> | PubMed
- [5] Xu Tonghui, Yu Xinzhu, Perlik Andrew J., Tobin Willie F., Zweig Jonathan A., Tennant Kelly, Jones Theresa, Zuo Yi (2009) Rapid formation and selective stabilization of synapses for enduring motor memories. *Nature* **462**:915-919 <https://doi.org/10.1038/nature08389> | PubMed
- [6] Hosp Jonas A., Pekanovic Ana, Rioult-Pedotti Mengia S., Luft Andreas R. (2011) Dopaminergic projections from midbrain to primary motor cortex mediate motor skill learning. *The Journal of Neuroscience* **31**:2481-2487 <https://doi.org/10.1523/jneurosci.5411-10.2011> | PubMed
- [7] Kawai Risa, Markman Timothy, Poddar Rajesh, Ko Raymond, Fantana Antoniu L., Dhawale Ashesh K., Kampff Adam R., Álvarez-Benito Bence P. (2015) Motor cortex is required for learning but not for executing a motor skill. *Neuron* **86**:800-812 <https://doi.org/10.1016/j.neuron.2015.03.024> | PubMed
- [8] Guo Jian-Zhong, Graves Austin R, Guo Wendy W, Zheng Jihong, Lee Allen, Rodríguez-González Juan, Li Nuo, Macklin John J, Phillips James W, Mensh Brett D, et al. (2015) Cortex commands the performance of skilled movement. *eLife* **4**:e10774 <https://doi.org/10.7554/eLife.10774> | PubMed
- [9] Markram Henry, Toledo-Rodriguez Maria, Wang Yun, Gupta Anirudh, Silberberg Gilad, Wu Caizhi (2004) Interneurons of the neocortical inhibitory system. *Nature Reviews Neuroscience* **5**:793-807 <https://doi.org/10.1038/nrn1519> | PubMed
- [10] Goldberg Jesse H., Lacefield Clay O., Yuste Rafael (2004) Global dendritic calcium spikes in mouse layer 5 low threshold spiking interneurons: implications for control of pyramidal cell bursting. *The Journal of Physiology* **558**:465-478 <https://doi.org/10.1113/jphysiol.2004.064519> | PubMed
- [11] Adler Avital, Zhao Ruohe, Shin Myung Eun, Yasuda Ryohei, Gan Wen-Biao (2019) Somatostatin-expressing interneurons enable and maintain learning-dependent sequential activation of pyramidal neurons. *Neuron* **102**:202-216.e7, <https://doi.org/10.1016/j.neuron.2019.01.036> | PubMed
- [12] Okoro Sandra U., Goz Roman U., Njeri Brigdet W., Harish Madhumita, Ruff Catherine F., Ross Sarah E., Gerfen Charles, Hooks Bryan M. (2022) Organization of cortical and thalamic input to inhibitory neurons in mouse motor cortex. *The Journal of Neuroscience* **42**:8095-8112 <https://doi.org/10.1523/jneurosci.0950-22.2022> | PubMed
- [13] Murayama Masanori, Enrique Pérez-Garci, Nevia Thomas, Bock Tobias, Senn Walter, Larkum Matthew E. (2009) Dendritic encoding of sensory stimuli controlled by deep cortical interneurons. *Nature* **457**:1137-1141 <https://doi.org/10.1038/nature07663> | PubMed
- [14] Kapfer Christoph, Glickfeld Lindsey L, Atallah Bassam V, Scanziani Massimo (2007) Supralinear increase of recurrent inhibition during sparse activity in the somatosensory cortex. *Nature Neuroscience* **10**:743-753 <https://doi.org/10.1038/nn1909> | PubMed
- [15] Silberberg Gilad, Markram Henry (2007) Disynaptic inhibition between neocortical pyramidal cells mediated by martinotti cells. *Neuron* **53**:735-746 <https://doi.org/10.1016/j.neuron.2007.02.012> | PubMed
- [16] Muñoz William, Tremblay Robin, Levenstein Daniel, Rudy Bernardo (2017) Layer-specific modulation of neocortical dendritic inhibition during active wakefulness. *Science* **355**:954-959 <https://doi.org/10.1126/science.aag2599> | PubMed
- [17] Riedemann Therese (2019) Diversity and function of somatostatin-expressing interneurons in the cerebral cortex. *International Journal of Molecular Sciences* **20**:2952 <https://doi.org/10.3390/ijms20122952> | PubMed
- [18] McGarry (2010) Quantitative classification of somatostatin-positive neocortical interneurons identifies three interneuron subtypes. *Frontiers in Neural Circuits* <https://doi.org/10.3389/fncir.2010.00012> | PubMed
- [19] Wang Yun, Toledo-Rodriguez Maria, Gupta Anirudh, Wu Caizhi, Silberberg Gilad, Luo Junyi, Markram Henry (2004) Anatomical, physiological and molecular properties of martinotti cells in the somatosensory cortex of the juvenile rat. *The Journal of Physiology* **561**:65-90 <https://doi.org/10.1113/jphysiol.2004.073353> | PubMed

- [20] **Gouwens Nathan W.**, Sorensen Staci A., Baftizadeh Fahimeh, Budzillo Agata, Lee Brian R., Jarsky Tim, Alfiler Lauren, Baker Katherine, Barkan Eliza, Berry Kyla, *et al.* (2020) Integrated morphoelectric and transcriptomic classification of cortical gabaergic cells. *Cell* **183**:935-953.e19, <https://doi.org/10.1016/j.cell.2020.09.057> | PubMed
- [21] **Wu Sherry Jingjing**, Sevier Elaine, Dwivedi Deepanjali, Saldi Giuseppe-Antonio, Hairston Ariel, Yu Sabrina, Abbott Lydia, Choi Da Hae, Sherer Mia, Qiu Yanjie, *et al.* (2023) Cortical somatostatin interneuron subtypes form cell-type-specific circuits. *Neuron* **111**:2675-2692.e9, <https://doi.org/10.1016/j.neuron.2023.05.032> | PubMed
- [22] **Xu Han**, Jeong Hyo-Young, Tremblay Robin, Rudy Bernardo (2013) Neocortical somatostatin-expressing gabaergic interneurons disinhibit the thalamorecipient layer 4. *Neuron* **77**:155-167 <https://doi.org/10.1016/j.neuron.2012.11.004> | PubMed
- [23] **Ma Zhengyu**, Liu Haixin, Komiyama Takaki, Wessel Ralf (2020) Stability of motor cortex network states during learning-associated neural reorganizations. *Journal of Neurophysiology* **124**:1327-1342 <https://doi.org/10.1152/jn.00061.2020> | PubMed
- [24] **Hilscher Markus M.**, Leão Richardson N., Edwards Steven J., Leão Katarina E., Kullander Klas (2017) ChRNA2-martinotti cells synchronize layer 5 type a pyramidal cells via rebound excitation. *PLOS Biology* **15**:e2001392 <https://doi.org/10.1371/journal.pbio.2001392> | PubMed
- [25] **Leão Richardson N.**, Mikulovic Sanja, Leão Katarina E, Munguba Hermany, Gezelius Henrik, Enjin Anders, Patra Kalicharan, Eriksson Anders, Loew Leslie M, Tort Adriano B L, *et al.* (2012) OLM interneurons differentially modulate CA3 and entorhinal inputs to hippocampal CA1 neurons. *Nature Neuroscience* **15**:1524-1530 <https://doi.org/10.1038/nn.3235> | PubMed
- [26] **Madisen Linda**, Zwingman Theresa A, Sunkin Susan M, Oh Seung Wook, Zariwala Hatim A, Gu Hong, Ng Lydia L, Palmiter Richard D, Hawrylycz Michael J, Jones Allan R, *et al.* (2009) A robust and high-throughput cre reporting and characterization system for the whole mouse brain. *Nature Neuroscience* **13**:133-140 <https://doi.org/10.1038/nn.2467> | PubMed
- [27] **Sousa Vitor H.**, Miyoshi Goichi, Hjerling-Leffler Jens, Karayannis Theofanis, Fishell Gord (2009) Characterization of nkx62-derived neocortical interneuron lineages. *Cerebral Cortex* **19**:10 <https://doi.org/10.1093/cercor/bhp038> | PubMed
- [28] **Paxinos George**, Franklin Keith BJ (2019) *Paxinos and Franklin's the mouse brain in stereotaxic coordinates* Academic press.
- [29] **Wang Xuhua**, Liu Yuanyuan, Li Xinjian, Zhang Zicong, Yang Hengfu, Zhang Yu, Williams Philip R., Alwahab Noaf S.A., Kapur Kush, Zhang Yiming, *et al.* (2017) Deconstruction of corticospinal circuits for goaldirected motor skills. *Cell* **171**:440-455.e14, <https://doi.org/10.1016/j.cell.2017.08.014> | PubMed
- [30] **Tennant Kelly A.**, Adkins DeAnna L., Donlan Nicole A., Asay Aaron L., Thomas Nagheme, Kleim Jeffrey A., Jones Theresa A. (2010) The organization of the forelimb representation of the c57bl/6 mouse motor cortex as defined by intracortical microstimulation and cytoarchitecture. *Cerebral Cortex* **21**:865-876 <https://doi.org/10.1093/cercor/bhq159> | PubMed
- [31] **Gomez Juan L.**, Bonaventura Jordi, Lesniak Wojciech, Mathews William B., Sysa-Shah Polina, Rodriguez Lionel A., Ellis Randall J., Richie Christopher T., Harvey Brandon K., Dannals Robert F., *et al.* (2017) Chemogenetics revealed: DREADD occupancy and activation via converted clozapine. *Science* **357**:503-507 <https://doi.org/10.1126/science.aan2475> | PubMed
- [32] **Manvich Daniel F.**, Webster Kevin A., Foster Stephanie L., Farrell Martilias S., Ritchie James C., Porter Joseph H., Weinshenker David (2018) The DREADD agonist clozapine noxide (cno) is reverse-metabolized to clozapine and produces clozapine-like interoceptive stimulus effects in rats and mice. *Scientific Reports* **8** <https://doi.org/10.1038/s41598-018-22116-z> | PubMed
- [33] **Couchman Lewis**, Morgan Phillip Edgar, Spencer Edgar Pathrose, Flanagan Robert James (2010) Plasma clozapine, norclozapine, and the clozapine: norclozapine ratio in relation to prescribed dose and other factors: data from a therapeutic drug monitoring service, 1993–2007. *Therapeutic drug monitoring* **32**:438-447 <https://doi.org/10.1097/FTD.0b013e3181dad1fb> | PubMed

- [34] **Albarran Eddy**, Raissi Aram, Jáidar Omar, Shatz Carla J., Ding Jun B. (2021) Enhancing motor learning by increasing the stability of newly formed dendritic spines in the motor cortex. *Neuron* **109**:3298-3311.e4. <https://doi.org/10.1016/j.neuron.2021.07.030> | [PubMed](#)
- [35] **Schindelin Johannes**, Arganda-Carreras Ignacio, Frise Erwin, Kaynig Verena, Longair Mark, Pietzsch Tobias, Preibisch Stephan, Rueden Curtis, Saalfeld Stephan, Schmid Benjamin, *et al.* (2012) Fiji: an open-source platform for biological-image analysis. *Nature Methods* **9**:676-682 <https://doi.org/10.1038/nmeth.2019> | [PubMed](#)
- [36] **Chen Tsai-Wen**, Wardill Trevor J., Sun Yi, Pulver Stefan R., Renninger Sabine L., Baohan Amy, Schreiter Eric R., Kerr Rex A., Orger Michael B., Jayaraman Vivek, *et al.* (2013) Ultrasensitive fluorescent proteins for imaging neuronal activity. *Nature* **499**:295-300 <https://doi.org/10.1038/nature12354> | [PubMed](#)
- [37] **Nakai Junichi**, Ohkura Masamichi, Imoto Keiji (2001) A high signal-to-noise ca²⁺ probe composed of a single green fluorescent protein. *Nature Biotechnology* **19**:137-141 <https://doi.org/10.1038/84397> | [PubMed](#)
- [38] **Miyawaki Atsushi**, Llopis Juan, Heim Roger, McCaffery J Michael, Adams Joseph A, Ikura Mitsuhiro, Tsien Roger Y (1997) Fluorescent indicators for ca²⁺ based on green fluorescent proteins and calmodulin. *Nature* **388**:882-887 <https://doi.org/10.1038/42264> | [PubMed](#)
- [39] **Zhou Pengcheng**, Resendez Shanna L, Rodriguez-Romaguera Jose, Jimenez Jessica C, Neufeld Shay Q, Giovannucci Andrea, Friedrich Johannes, Pnevmatikakis Eftychios A, Stuber Garret D, Hen Rene, *et al.* (2018) Efficient and accurate extraction of in vivo calcium signals from microendo-scopic video data. *eLife* **7** <https://doi.org/10.7554/elife.28728> | [PubMed](#)
- [40] **Giovannucci Andrea**, Friedrich Johannes, Gunn Pat, Kalfon Jérémie, Brown Brandon L, Koay Sue Ann, Taxidis Jiannis, Najafi Farzaneh, Gauthier Jeffrey L, Zhou Pengcheng, *et al.* (2019) Caiman an open source tool for scalable calcium imaging data analysis. *eLife* **8** <https://doi.org/10.7554/elife.38173> | [PubMed](#)
- [41] **Lopes Vítor**, Santos dos, Ribeiro Sidarta, Tort Adriano B.L. (2013) Detecting cell assemblies in large neuronal populations. *Journal of Neuroscience Methods* **220**:149-166 <https://doi.org/10.1016/j.jneumeth.2013.04.010> | [PubMed](#)
- [42] **Mölter Jan**, Avitan Lilach, Goodhill Geoffrey J. (2018) Detecting neural assemblies in calcium imaging data. *BMC Biology* **16** <https://doi.org/10.1186/s12915-018-0606-4> | [PubMed](#)
- [43] **Noguchi Kimihiro**, Gel Yulia R., Brunner Edgar, Konietzschke Frank (2012) nparLD: An R software package for the nonparametric analysis of longitudinal data in factorial experiments. *Journal of Statistical Software* **50** <https://doi.org/10.18637/jss.v050.i12>
- [44] **Gorsuch Richard L**, Lehmann Curtis (2017) Chi-square and f ratio: Which should be used when?. *Journal of Methods and Measurement in the Social Sciences* **8**:58-71 <https://doi.org/10.2458/v8i2.22990>
- [45] **Siegle Joshua H**, Hale Gregory J, Newman Jonathan P, Voigts Jakob (2015) Neural ensemble communities: open-source approaches to hardware for large-scale electrophysiology. *Current Opinion in Neurobiology* **32**:53-59 <https://doi.org/10.1016/j.conb.2014.11.004> | [PubMed](#)
- [46] **Virtanen Pauli**, Gommers Ralf, Oliphant Travis E., Haberland Matt, Reddy Tyler, Cournapeau David, Burovski Evgeni, Peterson Pearu, Weckesser Warren, Bright Jonathan, *et al.* (2020) and SciPy 1.0 Contributors. SciPy 1.0: Fundamental Algorithms for Scientific Computing in Python. *Nature Methods* **17**:261-272 <https://doi.org/10.1038/s41592-019-0686-2> | [PubMed](#)
- [47] **Harris Charles R.**, Millman K. Jarrod, van der Walt Stéfan J, Gommers Ralf, Virtanen Pauli, Cournapeau David, Wieser Eric, Taylor Julian, Berg Sebastian, Smith Nathaniel J., *et al.* (2020) Array programming with NumPy. *Nature* **585**:357-362 <https://doi.org/10.1038/s41586-020-2649-2> | [PubMed](#)
- [48] **Malfatti Thawann**, Ciralli Barbara (2023) Sciscrpts: a python library for controlling devices, running experiments and analyzing data. Zenodo. <https://doi.org/10.5281/zenodo.4045872>
- [49] **Hunter John D.** (2007) Matplotlib: A 2d Graphics Environment. *Computing in Science & Engineering* **9**:90-95 <https://doi.org/10.1109/MCSE.2007.55>
- [50] **Inkscape Project** (2022) Inkscape. <https://inkscape.org>

- [51] Bradski G. (2000) The OpenCV Library. *Dr. Dobbs's Journal of Software Tools*
- [52] Nath Tanmay, Mathis Alexander, Chen An Chi, Patel Amir, Bethge Matthias, Mathis Mackenzie Weygandt (2019) Using deeplabcut for 3d markerless pose estimation across species and behaviors. *Nature protocols* **14**:2152-2176 <https://doi.org/10.1038/s41596-019-0176-0> | PubMed
- [53] Malfatti Thawann (2024) repository. M1 martinotti movement. git. <https://gitlab.com/malfatti/M1MartinottiOnMovement>
- [54] Sanes Jerome N., Donoghue John P. (2000) Plasticity and primary motor cortex. *Annual Review of Neuroscience* **23**:393-415 <https://doi.org/10.1146/annurev.neuro.23.1.393> | PubMed
- [55] Armbruster B. N., Li X., Pausch M. H., Herlitze S., Roth B. L. (2007) Evolving the lock to fit the key to create a family of g protein-coupled receptors potently activated by an inert ligand. *Proceedings of the National Academy of Sciences* **104**:5163-5168 <https://doi.org/10.1073/pnas.0700293104> | PubMed
- [56] Velica Anna, Henriksson Katharina, Malfatti Thawann, Ciralli Barbara, Nogueira Ingrid, Asimakidou Evridiki, Kullander Klas (2025) Layer-specific connectivity and functional interference of chrna2+ layer 5 martinotti cells in the primary motor cortex. *European Journal of Neuroscience* **61** <https://doi.org/10.1111/ejn.70086> | PubMed
- [57] Alexander Georgia M., Rogan Sarah C., Abbas Atheir I., Armbruster Blaine N., Pei Ying, Allen John A., Nonneman Randal J., Hartmann John, Moy Sheryl S., Nicoletis Miguel A., et al. (2009) Remote control of neuronal activity in transgenic mice expressing evolved g protein-coupled receptors. *Neuron* **63**:27-39 <https://doi.org/10.1016/j.neuron.2009.06.014> | PubMed
- [58] Morgan JI (1988) Calcium as a modulator of the immediate-early gene cascade in neurons. *Cell calcium* **9**:303-311 [https://doi.org/10.1016/0143-4160\(88\)90011-5](https://doi.org/10.1016/0143-4160(88)90011-5) | PubMed
- [59] Bullitt Elizabeth (1990) Expression of c-fos-like protein as a marker for neuronal activity following noxious stimulation in the rat. *Journal of Comparative Neurology* **296**:517-530 <https://doi.org/10.1002/cne.902960402> | PubMed
- [60] van de Kamp Cornelis, Zaal Frank T. J. M. (2007) Prehension is really reaching and grasping. *Experimental Brain Research* **182**:27-34 <https://doi.org/10.1007/s00221-007-0968-2> | PubMed
- [61] Chen Chia-Chien, Gilmore Anthony, Zuo Yi (2014) Study motor skill learning by single-pellet reaching tasks in mice. *Journal of Visualized Experiments* <https://doi.org/10.3791/51238> | PubMed
- [62] Azim Eiman, Jiang Juan, Alstermark Bror, Jessell Thomas M. (2014) Skilled reaching relies on a v2a propriospinal internal copy circuit. *Nature* **508**:357-363 <https://doi.org/10.1038/nature13021> | PubMed
- [63] Jung Juergen C., Mehta Amit D., Aksay Emre, Stepnoski Raymond, Schnitzer Mark J. (2004) In vivo mammalian brain imaging using one- and two-photon fluorescence microendoscopy. *Journal of Neurophysiology* **92**:3121-3133 <https://doi.org/10.1152/jn.00234.2004> | PubMed
- [64] Resendez Shanna L, Jennings Josh H, Ung Randall L, Namboodiri Vijay Mohan K, Zhou Zhe Charles, Otis James M, Nomura Hiroshi, McHenry Jenna A, Kosyk Oksana, Stuber Garret D (2016) Visualization of cortical, subcortical and deep brain neural circuit dynamics during naturalistic mammalian behavior with head-mounted microscopes and chronically implanted lenses. *Nature Protocols* **11**:566-597 <https://doi.org/10.1038/nprot.2016.021> | PubMed
- [65] Peters Andrew J., Chen Simon X., Komiyama Takaki (2014) Emergence of reproducible spatiotemporal activity during motor learning. *Nature* **510**:263-267 <https://doi.org/10.1038/nature13235> | PubMed
- [66] Mahan Margaret Y., Georgopoulos Apostolos P. (2013) Motor directional tuning across brain areas: directional resonance and the role of inhibition for directional accuracy. *Frontiers in Neural Circuits* **7**:92 <https://doi.org/10.3389/fncir.2013.00092> | PubMed
- [67] Georgopoulos Apostolos P, Carpenter Adam F (2015) Coding of movements in the motor cortex. *Current Opinion in Neurobiology* **33**:34-39 <https://doi.org/10.1016/j.conb.2015.01.012> | PubMed
- [68] Biane Jeremy S., Takashima Yoshio, Scanziani Massimo, Conner James M., Tuszynski Mark H. (2019) Reorganization of recurrent layer 5 corticospinal networks following adult motor training. *The Journal of Neuroscience* **39**:4684-4693 <https://doi.org/10.1523/jneurosci.3442-17.2019> | PubMed

- [69] Floyer-Lea A., Matthews P. M. (2005) Distinguishable brain activation networks for short- and long-term motor skill learning. *Journal of Neurophysiology* **94**:512-518 <https://doi.org/10.1152/jn.00717.2004> | PubMed
- [70] Ruan Jingsong, Yao Yao (2020) Behavioral tests in rodent models of stroke. *Brain Hemorrhages* **1**:171-184 <https://doi.org/10.1016/j.hest.2020.09.001> | PubMed
- [71] Ratliff Floyd, Knight BW, Toyoda Jun-ichi, Hartline HK (1967) Enhancement of flicker by lateral inhibition. *Science* **158**:392-393 <https://doi.org/10.1126/science.158.3799.392> | PubMed
- [72] Yao Zizhen, van Velthoven Cindy T.J., Nguyen Thuc Nghi, Goldy Jeff, Sedeno-Cortes Adriana E., Baftizadeh Fahimeh, Bertagnolli Darren, Casper Tamara, Chiang Megan, Crichton Kirsten, *et al.* (2021) A taxonomy of transcriptomic cell types across the isocortex and hippocampal formation. *Cell* **184**:3222-3241.e26 <https://doi.org/10.1016/j.cell.2021.04.021> | PubMed
- [73] Chen Naiyan, Sugihara Hiroki, Sur Mriganka (2015) An acetylcholine-activated microcircuit drives temporal dynamics of cortical activity. *Nature Neuroscience* **18**:892-902 <https://doi.org/10.1038/nn.4002> | PubMed
- [74] Yang Jungwoo, Serrano Pablo, Yin Xuming, Sun Xiaochen, Lin Yingxi, Chen Simon X. (2022) Functionally distinct npas4-expressing somatostatin interneuron ensembles critical for motor skill learning. *Neuron* **110**:3339-3355.e8, <https://doi.org/10.1016/j.neuron.2022.08.018> | PubMed
- [75] Karnani Mahesh M, Agetsuma Masakazu, Yuste Rafael (2014) A blanket of inhibition: functional inferences from dense inhibitory connectivity. *Current Opinion in Neurobiology* **26**:96-102 <https://doi.org/10.1016/j.conb.2013.12.015> | PubMed
- [76] Deolindo Camila S., Kunicki Ana C. B., da Silva Maria I., Brasil Fabrício Lima, Moiola Renan C. (2018) Neuronal assemblies evidence distributed interactions within a tactile discrimination task in rats. *Frontiers in Neural Circuits* **11** <https://doi.org/10.3389/fncir.2017.00114> | PubMed
- [77] Vítor Lopes-dos Santos, Conde-Ocazonez Sergio, Nicoletis Miguel A. L., Ribeiro Sidarta T., Tort Adriano B. L. (2011) Neuronal assembly detection and cell membership specification by principal component analysis. *PLoS ONE* **6**:e20996 <https://doi.org/10.1371/journal.pone.0020996> | PubMed
- [78] Russo Eleonora, Durstewitz Daniel (2017) Cell assemblies at multiple time scales with arbitrary lag constellations. *eLife* **6**:e19428 <https://doi.org/10.7554/eLife.19428> | PubMed
- [79] Sakurai Yoshio (1998) The search for cell assemblies in the working brain. *Behavioural Brain Research* **91**:1-13 [https://doi.org/10.1016/s0166-4328\(97\)00106-x](https://doi.org/10.1016/s0166-4328(97)00106-x) | PubMed
- [80] Ren Chi, Peng Kailong, Yang Ruize, Liu Weikang, Liu Chang, Komiyama Takaki (2022) Global and subtype-specific modulation of cortical inhibitory neurons regulated by acetylcholine during motor learning. *Neuron* **110**:2334-2350.e8, <https://doi.org/10.1016/j.neuron.2022.04.031> | PubMed
- [81] Masamizu Yoshito, Tanaka Yasuhiro R, Tanaka Yasuyo H, Hira Riichiro, Ohkubo Fuki, Kitamura Kazuo, Isomura Yoshikazu, Okada Takashi, Matsuzaki Masanori (2014) Two distinct layer-specific dynamics of cortical ensembles during learning of a motor task. *Nature Neuroscience* **17**:987-994 <https://doi.org/10.1038/nn.3739> | PubMed
- [82] Buzsáki György, Wang Xiao-Jing (2012) Mechanisms of gamma oscillations. *Annual Review of Neuroscience* **35**:203-225 <https://doi.org/10.1146/annurev-neuro-062111-150444> | PubMed
- [83] Takada Naoki, Pi Hyun Jae, Sousa Vitor H., Waters Jack, Fishell Gord, Kepecs Adam, Osten Pavel (2014) A developmental cell-type switch in cortical interneurons leads to a selective defect in cortical oscillations. *Nature Communications* **5** <https://doi.org/10.1038/ncomms6333> | PubMed
- [84] Antonoudiou Pantelis, Tan Yu Lin, Kontou Georgina, Upton Louise, Mann Edward O. (2020) Parvalbumin and somatostatin interneurons contribute to the generation of hippocampal gamma oscillations. *The Journal of Neuroscience* **40**:7668-7687 <https://doi.org/10.1523/jneurosci.0261-20.2020> | PubMed
- [85] Mehring Carsten, Rickert Jörn, Vaadia Eilon, de Oliveira Simone Cardoso, Aertsen Ad, Rotter Stefan (2003) Inference of hand movements from local field potentials in monkey motor cortex. *Nature Neuroscience* **6**:1253-1254 <https://doi.org/10.1038/nn1158> | PubMed

- [86] Rickert Jörn, de Oliveira Simone Cardoso, Vaadia Eilon, Aertsen Ad, Rotter Stefan, Mehring Carsten (2005) Encoding of movement direction in different frequency ranges of motor cortical local field potentials. *The Journal of Neuroscience* **25**:8815-8824 <https://doi.org/10.1523/jneurosci.0816-05.2005> | PubMed
- [87] Acharya Soumyadipta, Fifer Matthew S, Benz Heather L, Crone Nathan E, Thakor Nitish V (2010) Electrocorticographic amplitude predicts finger positions during slow grasping motions of the hand. *Journal of Neural Engineering* **7**:046002 <https://doi.org/10.1088/1741-2560/7/4/046002> | PubMed
- [88] Slutzky Marc W, Jordan Luke R, Lindberg Eric W, Lindsay Kevin E, Miller Lee E (2011) Decoding the rat forelimb movement direction from epidural and intracortical field potentials. *Journal of Neural Engineering* **8**:036013 <https://doi.org/10.1088/1741-2560/8/3/036013> | PubMed
- [89] Alexander Georgia M, Brown Logan Y, Farris Shannon, Lustberg Daniel, Pantazis Caroline, Gloss Bernd, Plummer Nicholas W, Jensen Patricia, Dudek Serena M (2018) Ca² neuronal activity controls hippocampal low gamma and ripple oscillations. *eLife* **7** <https://doi.org/10.7554/elife.38052> | PubMed
- [90] Mahler Stephen V., Brodnik Zachary D., Cox Brittney M., Buchta William C., Bentzley Brandon S., Quintanilla Julian, Cope Zackary A., Lin Edwin C., Riedy Matthew D., Scofield Michael D., *et al.* (2018) Chemogenetic manipulations of ventral tegmental area dopamine neurons reveal multifaceted roles in cocaine abuse. *The Journal of Neuroscience* **39**:503-518 <https://doi.org/10.1523/jneurosci.0537-18.2018> | PubMed
- [91] Weera Marcus M, Agoglia Abigail E, Douglass Eliza, Jiang Zhiying, Rajamanickam Shivakumar, Shackett Rosetta S, Herman Melissa A, Justice Nicholas J, Gilpin Nicholas W (2022) Generation of a crf1-cre transgenic rat and the role of central amygdala crf1 cells in nociception and anxiety-like behavior. *eLife* **11** <https://doi.org/10.7554/elife.67822> | PubMed

Peer reviews

Reviewer #1 (Public review):

In this study, the authors investigated a specific subtype of SST-INs (layer 5 ChRNA2-expressing Martinotti cells) and examined its functional role in motor learning.

Most of the issues remain unaddressed. The findings across experiments are inconsistent, and it is unclear how the authors performed their analyses or why specific time points and comparisons were chosen. The study will require major re-analyzing and additional experiments to substantiate its conclusions.

After reading the reviewers' responses, my major concerns about the manuscript remain unresolved, particularly regarding the arbitrarily defined stages of learning in the motor learning task and how the calcium imaging data align with the animal's movements.

- In line 331, the authors refer to session 5 as "training," describing it as the final spoon session, and session 6 as "re-training," because it is the first session in which the pellet is presented on the plate rather than on the spoon. However, in Fig. 1F-H, even in the Ctrl group, it is clear that the performance drops significantly in session 5, which is supposed to be the easiest session before switching to the more difficult plate condition.

- In the classic pellet-reaching task, the spoon sessions would typically be considered "shaping", while the plate sessions would represent the actual training phase. However, in this manuscript, the authors still insist on referring to session 2 as "learning" and session 5 as "training." I don't understand the difference between session 2 and session 5, especially when session 5's performance is lower than session 2 (even in Fig 1H when you compare succ ratio).

- Since session 6 (on the plate) is considered as "retraining," why don't the authors present the behavioral results beyond session 6? As a result, it remains unclear whether the animals improved their performance during the retraining phase.

- Lastly, in Fig. 4B the authors present only the success ratio and claim that performance improves with CLZ application. However, when comparing sessions 8-10 between the Ctrl and Cre⁺ groups, there already appears to be a baseline difference. CLZ treatment in Cre⁺ mice seem to bring performance only to the WT level rather than producing a clear improvement beyond baseline.

- Regarding the alignment between imaging and behavior, the authors report ~100 prehensions per minute. However, the calcium imaging traces show fewer than 20-30 spikes over 150 seconds (~2.5 min; Fig. 1E). This discrepancy raises concerns about whether the authors can truly isolate calcium signals corresponding to individual prehension events (either successful ones or multiple combined events for unsuccessful attempts). The manuscript still does not present behavioral data that directly aligns prehension events with calcium imaging activity. Although the authors performed analyses suggesting that prehension-related activity does not systematically alter non-prehension epochs, this claim is difficult to evaluate without seeing the underlying traces. It is therefore unclear how the authors selected the example calcium traces aligned to prehension onset, given that there are more than 100 prehension events per minute.

- In Fig. 1I, the authors also did not address why neural activity during successful trials is already lower one second before movement onset. The longer traces provided do not help to explain this observation or clarify the origin of this pre-movement reduction in activity. It actually further suggests that there may be some artifacts in the imaging that could affect the analysis.

- Overall, because it remains difficult to understand exactly what the authors are analyzing (and because the definitions of the motor learning stages appear arbitrary) it is difficult to agree with the authors' conclusion that Ma2s cells reduce PyrN cell assembly plasticity during learning, thereby possibly facilitating already acquired motor skills.

<https://doi.org/10.7554/eLife.109286.2.sa2>

Reviewer #2 (Public review):

Summary:

In this manuscript, Malfatti et al. study the role of ChRNA2 Martinotti cells (Ma2 cells), a subset of SST interneurons, for motor learning and motor cortex activity. The authors trained mice on a forelimb prehension task while recording neuronal activity of pyramidal cells using calcium imaging with a head mounted miniscope. While chemogenetically increasing Ma2 cell activity did not affect motor learning, it changed pyramidal cell activity such that activity peaks become sharper and differently timed than in control mice. Moreover, co-active neuronal assemblies become more stable with a smaller spatial distribution. Increasing Ma2 cell activity in previously trained mice did increase performance on the prehension task and led to increased theta and gamma band activity in the motor cortex. On the other hand, genetic ablation of Ma2 cells affected fine motor movements on a pasta handling task while not affecting the prehension task. While overall this study addresses an important and timely question, limitations in the design of the motor learning task and data analysis significantly weaken the conclusions drawn in this manuscript.

Strengths:

The proposed question of how *Chrna2*-expressing SST interneurons affect motor learning and motor cortex activity is important and timely. The study employs sophisticated approaches to record neuronal activity and manipulate the activity of a specific neuronal population in behaving mice over the course of motor learning. The authors analyze a variety of neuronal activity parameters, comparing different behavior trials, stages of learning, and the effects of *Ma2* cell activation. The analysis of neuronal assembly activity and stability over the course of learning by tracking individual neurons throughout the imaging sessions is notable, since technically challenging, and yielded the interesting result that neuronal assemblies are more stable when activating *Ma2* cells.

Overall, the study provides compelling evidence that *Ma2* cells regulate certain aspects of motor behaviors, likely by shaping circuit activity in the motor cortex.

Weaknesses:

While the authors addressed some of the concerns raised by the reviewers, several major limitations still exist in the revised manuscript.

(1) I appreciate the authors now showing more measures of the prehension task (total reaches, success reaches/min, and success ratio) and providing more details on the task design. However, it is unclear why the authors chose a task design that is somewhat different from the commonly used approach. Here they increase the distance of the food pellet each session and are thus making the task increasingly harder, whereas commonly the target distance is kept stable (See 10.1038/nature08389 for example). The result is that important readouts of learning (e. g. success rate) thus remain stable, making it impossible to judge if learning has occurred, without a control group of non-trained mice. This makes it impossible to judge if the task is affected by increased *Ma2* cell excitability, since there is no reference of how these measurements are supposed to change in a mouse that learns or doesn't learn the task.

(2) Regarding the analysis of the calcium imaging data, it is still unclear why the authors cannot report a commonly used dF/F_0 or z-score value, as recommended by both reviewers. The authors state the 1 sec time window prior to the prehension cannot be used as a baseline (F_0), as there might be preparatory motor activity. In that case an even earlier window (such as -2 to -1sec) or z-scores should be used. The current version relabeling the background subtracted fluorescence signal as dF/F_0 is misleading. Relatedly, it is unclear why the authors don't think the 1 sec window before prehension cannot be used as baseline, but at the same time use the difference in calcium activity before and after prehension onset as a cut-off criterion for defining cells as modulated during prehension and including in the analysis.

(3) While the authors have improved their statistical reporting, key information is still missing in several places. For example, no N-numbers are listed in legends for figure 3, and there is no mention of the number of mice for analysis in figures 2 and 3. For clarity, the authors should also include the statistical test performed in the figure legends for any p-values shown in the figure.

<https://doi.org/10.7554/eLife.109286.2.sa1>

Author Response:

The following is the authors' response to the original reviews.

eLife Assessment

This valuable study addresses a critical and timely question regarding the role of a subpopulation of cortical interneurons (Chrna2-expressing Martinotti cells) in motor learning and cortical dynamics. However, while some of the behavior and imaging data

are impressive, the small sample sizes and incomplete behavioral and activity analyses make interpretation difficult; therefore, they are insufficient to support the central conclusions. The study may be of interest to neuroscientists studying cortical neural circuits, motor learning, and motor control.

We thank the reviewers and the editors for the insightful comments. We are pleased to report that the raised issues with the manuscript can be addressed by improving clarity in our writing of specific sections and by providing additional analysis. Specifically, it was not clear in the manuscript text that although we show illustrative data with a lower number of animals, our conclusions are supported by data with a larger and sufficient sample size. Also, the description of our control experiments has been improved to clarify our proper treatment controls. We therefore clarify below that our study presents compelling and sufficient evidence to support our conclusions. We have responded to all the comments, explaining how each concern has been addressed. All line and figure numbers mentioned here refer to the numbering of the reviewed manuscript version. All references are cited as DOIs.

Reviewer #1 (Public review):

There are many major issues with the study. The findings across experiments are inconsistent, and it is unclear how the authors performed their analyses or why specific time points and comparisons were chosen. The study requires major re-analysis and additional experiments to substantiate its conclusions.

The main limitation of the study lies in its small sample sizes and the absence of key control experiments, which substantially weaken the strength of the conclusions.

(1a) Behavior task - the pellet-reaching task is a well-established paradigm in the motor learning field. Why did the authors choose to quantify performance using "success pellets per minute" instead of the more conventional "success rate" (see PMID 19946267, 31901303, 34437845, 24805237)? It is also confusing that the authors describe sessions 1-5 as being performed on a spoon, while from session 6 onward, the pellets are presented on a plate. However, in lines 710-713, the authors define session 1 as "naive," session 2 as "learning," session 5 as "training," and "retraining" as a condition in which a more challenging pellet presentation was introduced. Does "naive session 1" refer to the first spoon session or to session 6 (when the food is presented on a plate)? The same ambiguity applies to "learning session 2," "training session 5," and so on. Furthermore, what criteria did the authors use to designate specific sessions as "learning" versus "training"? Are these definitions based on behavioral performance thresholds or some biological mechanisms? Clarifying these distinctions is essential for interpreting the behavioral results.

We agree that success rate is a more conventional measure than the number of successful prehensions per minute. We have changed all behavior quantifications to success rate. Note that all behavioral conclusions drawn before are still valid under the new quantification (see Figures 1, 4, and 5). Importantly, the terms "learning," "training," and "retraining" were defined based on task structure and prior literature on motor learning stages rather than predetermined behavioral performance thresholds. These labels reflect progression through the task design (initial acquisition, continued practice under stable conditions, and adaptation to altered task demands), not biologically distinct or threshold-defined phases. We have revised the Methods section to make these definitions and transitions explicit to avoid ambiguity in interpreting the behavioral results.

(1b) Judging from Figures 1F and 4B, even in WT mice, it is not convincing that the animals have actually learned the task. In all figures, the mice generally achieve 10-20 pellets per minute across sessions. The only sessions showing slightly higher

performance are session 5 in Figure 1F ("train") and sessions 12 and 13 in Figure 4B ("CLZ"). In the classical pellet-reaching task, animals are typically trained for 10-12 sessions (approximately 60 trials per session, one session per day), and a clear performance improvement is observed over time. The authors should therefore present performance data for each individual session to determine whether there is any consistent improvement across days. As currently shown, performance appears largely unchanged across sessions, raising doubts about whether motor learning actually occurred.

As described in the methods Single pellet prehension task section, in our setup box, the elevated plate slot for pellet delivery is at a challenging position, outside the slit and 2cm to the right, forcing the mice to use the left paw. Therefore, mice need to be trained in gradually harder positions, using a spoon to deliver the pellet instead of placing it directly at the plate slot. Due to the gradually increasing difficulty in the task, the success rate curve remains flat, while the total number of attempts and number of successful prehensions per minute increase (Figure 1 F-H). We therefore argue that motor learning indeed occurred, with a relatively constant success rate when performing a gradually harder task. Further, the success rate and number of successful prehensions of our mice is within levels previously reported for trained mice (10.3791/51238). We added the precise plate slot position in the methods section to make clearer the need of a gradually increasing difficulty delivery method.

(1c) The authors also appear to neglect existing literature on the role of SST-INs in motor learning and local circuit plasticity (e.g., PMID 26098758, 36099920). Although the current study focuses on a specific subpopulation of SST-INs, the results reported here are entirely opposite to those of previous studies. The authors should, at a minimum, acknowledge these discrepancies and discuss potential reasons for the differing outcomes in the Discussion section.

We thank the reviewer for pointing this out. It is by no means a neglect, but a careful balance discussing previous literature that can be fairly compared with our findings. It is becoming increasingly clear — with mounting evidence from modern transcriptomic and connectomic studies — that the canonical “three-cardinal” interneuron populations (SST⁺, PV⁺, VIP⁺) represent oversimplified groupings that mask considerable heterogeneity. For example, in a comprehensive single-cell RNA-sequencing (scRNA-seq) study covering ~1.3 million cells from mouse cortex and hippocampus, the authors identified dozens of discrete GABAergic subtypes beyond the classical marker-defined classes, revealing continuous and graded variation in molecular identity across cortical and hippocampal regions (10.1016/j.cell.2021.04.021). Moreover, a recent study focusing on SST-expressing interneurons demonstrated that even within the SST class there are multiple subtypes with distinct laminar distributions, axonal projection patterns, and circuit connectivity — for instance, two different Martinotti subtypes vs. a non-Martinotti SST subtype targeting different pyramidal neuron types and dendritic compartments (10.1016/j.neuron.2023.05.032). Finally, developmental single-cell transcriptomics shows that interneuron diversity is already apparent at early postmitotic stages, indicating that these subtypes are pre-specified rather than being mere activity-dependent states (10.1038/s41467-018-07458-1). These findings argue strongly that the traditional SST⁺ / PV⁺ / VIP⁺ classification, while useful as a coarse heuristic, fails to capture the rich diversity in molecular, morphological, and functional phenotypes that likely underlie distinct roles in circuit computation and behavior.

The consequence of this is that studies using any of these three markers must be cautiously interpreted since in reality, several quite different neuronal populations are studied at once, especially if no efforts were made to tease out which of the participating populations (inside the “cardinal” population) contribute to the effects seen. Most likely, the reported results are

based on a mixed population - in the worst case scenario - populations with opposite effects. In any case, we have now included the role of SST-INs in motor learning and M1 circuitry in the discussion section. We also respectfully disagree that our findings are the opposite of previous SST-IN studies. We show that increasing Ma2 excitability improved execution of an already learned movement, while 10.1038/nn.4049 showed that both activating (which is different from increasing excitability) and inhibiting SST-INs impaired the learning of a stereotyped movement. Similarly, 10.1016/j.neuron.2022.08.018 showed that increasing SST-INs excitability impairs motor learning, not execution of a previously learned movement. While we found that increasing excitability of Ma2 cells did not affect motor learning, note that the Ma2 are a subset of martinotti cells with homogeneous electrophysiological and morphological properties (10.1371/journal.pbio.2001392), and martinotti cells themselves are a subset of SST+ cells (10.1016/j.neuron.2023.05.032). The discussion has been updated to include this reasoning.

(2a) Calcium imaging - The methodology for quantifying fluorescence changes is confusing and insufficiently described. The use of absolute dF values ("detrended by baseline subtraction," lines 565-567) for analyses that compare activity across cells and animals (e.g., Figure 1H) is highly unconventional and problematic. Calcium imaging is typically reported as dF/F0 or z-scores to account for large variations in baseline fluorescence (F0) due to differences in GCaMP expression, cell size, and imaging quality. Absolute dF values are uninterpretable without reference to baseline intensity - for example, a dF of 5 corresponds to a 100% change in a dim cell (F0 = 5) but only a 1% change in a bright cell (F0 = 500). This issue could confound all subsequent population-level analyses (e.g., mean or median activity) and across-group comparisons. Moreover, while some figures indicate that normalization was performed, the Methods section lacks any detailed description of how this normalization was implemented. The critical parameters used to define the baseline are also omitted. The authors should reprocess the imaging data using a standardized dF/F0 or z-score approach, explicitly define the baseline calculation procedure, and revise all related figures and statistical analyses accordingly.

The calcium imaging used here is 1-photon microendoscopic video data. To our knowledge, it is not possible to extract the true cell baseline over time from 1-photon data, since the background component includes signals from multiple sources, and usually has fluctuations larger than the neural signal itself. We agree that absolute dF values cannot be compared across cells, and that is not what we report here. The CNMF-E algorithm outputs the temporal activity of each neuron with the background component already removed (10.7554/eLife.28728) and therefore the baseline subtraction used in our study is already standardized (10.7554/eLife.38173). Note that although it is common in the literature to record 1-photon data and perform similar preprocessing (some form of baseline subtraction and/or normalization by noise std), referring to the resulting trace as dF/F, that is not entirely correct, since true F0 extraction is not possible. We thus chose to refer to the resulting preprocessed traces as what they actually are - dF detrended (raw trace with estimated background components removed). However, we agree that a better description of the process would be helpful in our manuscript, and that the nomenclature might be confusing to readers. We therefore expanded the methods section to better explain that we will now refer to F0 as the background component (and refer to our resulting traces as dF/F) and explain how it was determined. We also updated the example traces in Figure 1E to now show the raw traces, the estimated background components and the detrended traces.

(2b) Figure 1G - It is unclear why neural activity during successful trials is already lower one second before movement onset. Full traces with longer duration before and after movement onset should also be shown. Additionally, only data from "session 2 (learning)" and a single neuron are presented. The authors should present data across

all sessions and multiple neurons to determine whether this observation is consistent and whether it depends on the stage of learning.

We agree that it would be beneficial to show longer traces as an example of prehension-related activity, so we expanded Figure 1I to show a longer trace for a single neuron. We added to Supplemental Figure 2 plots showing longer traces from all sessions including all neurons for both genotypes.

(2c) Figure 1H - The authors report that chemogenetic activation of Chrna2 cells induces differential changes in PyrN activity between successful and failed trials. However, one would expect that activating all Chrna2 cells would strongly suppress PyrN activity rather than amplifying the activity differences between trials. The authors should clarify the mechanism by which Chrna2 cell activation could exaggerate the divergence in PyrN responses between successful and failed trials. Perhaps, performing calcium imaging of Chrna2 cells themselves during successful versus failed trials would provide insight into their endogenous activity patterns and help interpret how their activation influences PyrN activity during successful and failed trials.

The reviewer is correct to assume that increasing excitability of Ma2 cells would suppress PC activity. As shown in Supplemental Figure 2I, that is exactly what we observe when considering only non-prehension related activity. Thus, it is very interesting that the opposite effect is seen for prehension-related activity. Also, this finding perfectly aligns with our results from the assembly analysis showing that assembly activity is decreased within the prehension window compared to outside the prehension window. Unfortunately, imaging Ma2 cells would only add information to this study in understanding their influence on PCs if we image both populations simultaneously, which require equipment and reagents we do not currently have. Fortunately, however, the endogenous activity patterns of Ma2 cells and the direct connectivity between Ma2 and pyramidal cells was already previously investigated in detail (10.1371/journal.pbio.2001392), therefore we expanded the discussion to better explain that the differential changes in PC when increasing Ma2 excitability could be due to increased PC synchronization, since a single Ma2 connects to several PCs, and upon inhibition release all connected PCs fire synchronously.

(2d) Figure 1H - Also, in general, the Cre+ (red) data points appear consistently higher in activity than the Cre- (black) points. This is counterintuitive, as activating Chrna2 cells should enhance inhibition and thereby reduce PyrN activity. The authors should clarify how Cre+ animals exhibit higher overall PyrN activity under a manipulation expected to suppress it. This discrepancy raises concerns about the interpretation of the chemogenetic activation effects and the underlying circuit logic.

As explained above, increasing Ma2 excitability indeed decreased non-prehension related PC activity, and the proposed mechanism has been added to the discussion section. We also made

clearer in the results section that we are referring to prehension-related PC activity, and emphasize that overall non-prehension related PC activity is decreased.

(3) The statistical comparisons throughout the manuscript are confusing. In many cases, the authors appear to perform multiple comparisons only among the N, L, T, and R conditions within the WT group. However, the central goal of this study should be to assess differences between the WT and hM3D groups. In fact, it is unclear why the authors only provide p-values for some comparisons but not for the majority of the groups.

We agree that a clearer description of the statistical analysis is warranted. We expanded the statistical analysis methods section to clarify, among other things, that all possible pairwise

comparisons were performed and appropriately corrected for multiple comparisons, and only positive p-values are reported in the figures, therefore the absence of p-value for a comparison means that is not significant.

(4a) Figure 4 - It is hard to understand why the authors introduce LFP experiments here, and the results are difficult to interpret in isolation. The authors should consider combining LFP recordings with calcium imaging (as in Figure 1) or, alternatively, repeating calcium imaging throughout the entire re-training period. This would provide a clearer link between circuit activity and behavior and strengthen the conclusions regarding Chrna2 cell function during re-training.

Unfortunately, it is not possible in our setup to record calcium imaging and LFP simultaneously, since the implants needed for the miniscope occupy the entire space above the animal's cranium. To record calcium imaging during the execution of learned movements is also impractical. If the animals were to be implanted before the training phase, the signal will likely be too degraded for recordings after the training sessions, since the miniscope signal quality decreases over time, and over successive miniscope attachments. If the animals were to be implanted between the training and retraining phase (as the LFP group), the gap between training and retraining would be even larger, at least 28 days (as opposed to 16 days for the LFP group), which would affect the performance in the task. Therefore, LFP recordings provide understanding of the higher-level changes happening in neural activity when excitation is increased in Ma2 cells during the execution of learned movements. We respectfully disagree that the results from the LFP group cannot be interpreted in isolation, since we found that mice with increased excitability of Ma2 cells display increased low theta and gamma power during the prehension movement. As discussed in the manuscript, the increased high gamma band power when Ma2 cells are overexcitable, particularly for the successful trials in the planning phase, suggest that Ma2 cells may have a role influencing theta and gamma oscillations during motor performance (lines 1348-1355).

(4b) It is unclear why CLZ has no apparent effect in session 11, yet induces a large performance increase in sessions 12 and 13. Even then, the performance in sessions 12 and 13 (30 successful pellets) is roughly comparable to Session 5 in Figure 1F. Given this, it is questionable whether the authors can conclude that Chrna2 cell activation truly facilitates previously acquired motor skills?

We understand that a source of confusion for the behavioral data in the LFP group was the absence of data from sessions 1-7, together with the missing explanation about the task changing from spoon to plate (as explained in answers to question 1a and 1b). Since the animals are getting pellets from the spoon in session 5 (easier) and from the plate in later sessions (harder), the fact that animals achieved the same performance in the plate as they had on the last spoon session indicates they relearned the movement. To further clarify the training development, we added the full set of sessions (1-13) to Supplemental Figure 7, indicating the spoon-to-plate switch after session 5 and the 16-days gap between sessions 7 and 8 (due to viral injection and electrodes implant surgeries).

(5) Figure 5 - The authors report decreased performance in the pasta-handling task (presumably representing a newly learned skill) but observe no difference in the pellet-reaching task (presumably an already acquired skill). This appears to contradict the authors' main claim that Chrna2 cell activation facilitates previously acquired motor skills.

We respectfully disagree that the results for the pasta-handling conflict with the finding that increasing Ma2 excitability facilitates previously acquired movements. The pasta handling specifically measures forepaw dexterity (as outlined in lines 442-444), therefore assessing forelimb function unrelated to learning. Mice perform a set of stereotyped movements to manipulate the pasta, therefore no learning is required (note that animals were habituated to

the arena, followed by a single test session, with no training sessions). We do specifically mention in the results section that "we used the pasta handling task to assess forepaw dexterity that does not require learning" (lines 1137-1139). Our findings support our reported conclusion that "Ma2 cells may have a role in orchestrating precise forelimb movements that do not require previous specific training" (lines 1154-1156).

(6) Supplementary Figure 1 - The c-Fos staining appears unusually clean. Previous studies have shown that even in home-cage mice, there are substantial numbers of c-Fos+ cells in M1 under basal conditions (PMID 31901303, 31901303). Additionally, the authors should present Chrna2 cell labeling and c-Fos staining in separate channels. As currently shown, it is difficult to determine whether the c-Fos+ cells are truly Chrna2+ cells.

Our c-Fos stain does work well after having improved this method in several of our projects. Unfortunately, we could not check the references mentioned in the comment, since it points to a study that did not mention c-Fos (maybe incorrect PMID code?). However, we found our images to have similar c-Fos levels in control as other studies (for example 10.3389/fnana.2014.00013 Figure 1A and 10.1109/TBME.2024.3401136 Supplemental Figure 2C). Thus, we do find background activity of c-Fos in both Cre+ and control mice, but the c-Fos stain appears clean because of the strong up-regulation and fluorescent signal in exogenously activated hM3Dq+ cells. Also, we noticed that the manuscript was missing a methods section for the c-Fos experiments, therefore we added a section detailing the hM3Dq activation validation (lines 487-498). Further, the figure now displays separate channels for hM3Dq + cells (magenta) and c-Fos (cyan) for better clarity.

(7) Overall, the authors selectively report statistical comparisons only for findings that support their claims, while most other potentially informative comparisons are omitted. Complete and transparent reporting is necessary for proper interpretation of the data.

As explained above (comment 3), we expanded the statistical description in the methods to explain that all possible pairwise comparisons were performed and appropriately corrected for multiple comparisons, and that omitted comparisons are non-significant.

Reviewer #1 (Recommendations for the authors):

(1) Figure legends - The authors should provide more detailed information in the figure legends, such as N values. It is also not explained what the bold bars, as well as the highest and lowest bars, represent. Clear labeling is essential for proper interpretation of the data.

We revised all figure legends to add n-numbers for all quantification plots, and expanded the Statistical analysis methods section to explain the labeling of all quantifications.

(2) Presentation of plots - The authors need to improve the clarity and completeness of their figure presentations. For example:

(a) In Figure 1F, it is unclear whether the results were obtained under chemogenetic activation, as this information is missing from both the figure and the legend. Currently, it could be a comparison of Cre+ mice with Cre- mice without any manipulations.

(b) In Figure 1H, p-values are reported, but it is not specified which groups are being compared. As mentioned above, why are p-values only given to some comparisons? Does that mean the others are not significant?

(c) In Figure 1D, a scale bar should be provided.

(d) In Figure 1E, the y-axis (fluorescence) scale should be clearly indicated.

We thank the reviewer's attention to the figure details. We added the missing scale bars for Figures 1D-E. We also clarified in the results section that all miniscope recordings were performed under clozapine treatment. As answered above (comments 3 and 7), we expanded the methods section to state that although all comparisons were made and appropriately corrected for multiple comparisons, only significant comparisons were reported. As for the groups being compared, every significance bar clearly connects two groups, which are the ones being compared. We also expanded the Statistical Analysis section to state that "Significance bars without ticks represent pairwise comparisons, while significance bars with downward ticks represent an effect."

Reviewer #2 (Public review):

The main limitation of the study lies in its small sample sizes and the absence of key control experiments, which substantially weaken the strength of the conclusions. Core findings of this paper, such as the lack of effect of Ma2 cell activation on motor learning, as well as the altered neuronal activity, rely on a sample size of n=3 mice per condition, which is likely underpowered to detect differences in behavior and contributes to the somewhat disconnected results on calcium activity, activity timing, and neuronal assembly activity.

We understand that the source of confusion is the number of mice used for calcium imaging and the number of mice used for assessing the effect of Ma2 increased excitability in motor learning. The core finding that Ma2 increased excitability did not alter motor learning is supported by the data shown previously in Supplemental Figure 5 (now Figure 1F-H), with n=6 Cre⁺ and n=7 controls, which has enough statistical power to detect the effect of training session ($F(3,33) = 9.254$, power = 0.997) and should have enough power to detect the effect of group (estimated power of 0.835 for $F(1,11)$). The behavior performance of the miniscope-recorded mice was shown in the previous version for transparency, however no conclusion was drawn based on that data. To improve clarity, we now present data from the previous Supplemental Figure 5 as Figures 1F-H. This dataset clearly demonstrates that increased excitability of Ma2 cells did not affect motor learning. In addition, note that all quantification and conclusions drawn about neuronal activity are based on robust sample sizes: 1070 cells for controls and 403 for Chrna2-Cre⁺, or 70 assemblies for controls and 48 for Chrna2-Cre⁺. These sample sizes ensure sufficient statistical power, as demonstrated by the multiple significant effects and pairwise differences reported in our study. We reiterate that no underpowered tests were conducted in this study, and no conclusions were drawn on n = 3 controls and 3 Chrna2-Cre⁺ mice on behavioral outcomes.

More comprehensive analyses and data presentation are also needed to substantiate the results. For example, examining calcium activity and behavioral performance on a trial-by-trial basis could clarify whether closely spaced reaching attempts influence baseline signals and skew interpretation.

We agree and we performed a trial-by-trial analysis to verify the effect of adjacent prehensions in the trial signal. We found that only 17.7% of adjacent trials were affected by a previous trial. In addition we selected only trials not preceded by another trial for at least 6s, and evaluated whether activity immediately before the trial (-3 to -1s) is different from the activity long before the trial (-5 to -3s). The rationale is that if a trial would affect the baseline, then activity immediately before would be different from the activity long before the trial. In this analysis, we found no genotype- or session-related differences in baseline amplitude between epochs. Together these results confirm that prehension-related activity does not systematically alter non-prehension epochs. The results are shown in Supplemental Figure 3.

The study uses cre-negative mice as controls for hM3Dq-mediated activation, which does not account for potential effects of Cre-dependent viral expression that occur only in Cre-

positive mice. This important control would be necessary to substantiate the conclusion that it is increased Ma2 cell activity that drives the observed changes in behavior and cortical activity.

Having a control group of Cre⁺ mice injected with cre-dependent vector control carrying, for example, only fluorescence, would add one more layer of certainty that the effects observed here are due to CLZ-induced hM3Dq activation. We do not agree, however, that it is necessary to confirm our findings. Cre-dependent expression alone was already extensively demonstrated to have no effect by comparing a DREADD activator to a vehicle treatment (for example 10.7554/eLife.38052, 10.1523/JNEUROSCI.0537-18.2018, 10.7554/eLife.67822). We also showed this for our LFP group (Figure 4), further confirming no effect of Cre-dependent hM3Dq expression alone.

An unspecific effect of clozapine, where the treatment affects animals without the hM3Dq receptor, would be much more likely. We do control for this by giving the same treatment to Cre⁺ and Cre⁻ mice. Moreover, since we use a low dose of clozapine, a lack of hM3Dq activation would be more likely, which we also controlled for with the c-Fos experiment as explained in the answer to the Minor point 1. Nevertheless, we added to the discussion that although we find it highly unlikely that the effects found here are due to Cre-dependent viral expression, we have not recorded Cre⁺ animals expressing control vectors instead of hM3Dq (lines 1360-1375).

Reviewer #2 (Recommendations for the authors):

Major points

(1) One of the main findings in this paper is that Chrna2-Cre cell activation did not affect learning of the prehension task; however, the presented data do not convincingly support this claim. Looking at Fig.1F, Cre⁺ mice appear to have an overall lower number of successful prehensions compared to control mice. If this is not statistically significant, it is likely because n=3 mice for each group is underpowered. To better judge the behavior of these mice, it would be necessary to plot success rate and overall number of prehensions over the entire course of training, in addition to successes per minute. Given that n=3, plotting all individual data points would make more sense than showing a violin plot. Relatedly, in Supplemental Figure 5, there appears to be a clear effect on reduced success rates in Cre⁺ mice, which is stated in the figure legends, whereas the result section states: we found no effect of genotype on prehension success rates (lines 895-896). The authors should ensure that these behavior experiments are sufficiently powered to detect potential differences in learning between groups and present the complete data and statistical analysis.

As explained on Comment 1, the finding that Ma2 increased excitability did not alter motor learning is not based on the data on the previous Figure 1F (n=3 Cre⁺ and n=3 controls, shown for transparency). Instead, it is supported by the data in the previous Supplemental Figure 5, now Figures 1F-H, with n=6 Cre⁺ and n=7 controls, for which we found only overall effects of training session, but no effect of genotype, with no significant post-hoc pairwise comparisons. We agree that plotting the success rate, total number of prehensions and successful prehensions per minute, for all 6 sessions, allows better evaluation of the mice behavior. We moved the Supplemental Figure 5 into Figure 1, plotting the three measures for the full set of sessions, with individual data points within the violin plots, and expanded the statistical results description on the main text. We reiterate that no underpowered tests were conducted in this study, and no conclusions were drawn on n = 3 controls and 3 Chrna2-Cre⁺ mice.

(2) The authors mention that a significant fraction of prehension trials overlapped with a preceding prehension attempt. Were those attempts excluded from the analysis? The

stark differences in calcium signals at baseline before prehension onset in some sessions (Figure 1G, Supplementary Figure 2D) suggest that trials preceding closely in time might play a role and could skew the analysis and interpretation.

Overlapping trials were not excluded from the previous analysis. As summarized in our response to Comment 2, and expanded in the results section (lines 876-894), we found that only 17.7% of adjacent trials were affected by a previous trial, and that when selecting only trials not preceded by another trial for at least 6s, we found no effect of prehension-related activity in the baseline preceding the trials.

(3) Relatedly, to test the differences in calcium activity before and after prehension onset, it would be clearer to use a delta F/F measure where the 1 second before onset is used as baseline.

Since a large proportion of neurons are more active before the onset (on the movement planning phase, Figure 2C), the activity 1s before the movement onset cannot be considered as F0. Dividing the activity during the movement by the activity during the planning phase would generate a different measure, a form of execution/planning ratio. We performed this analysis as an additional measure and found a three-way interaction effect of genotype, session, and prehension accuracy, driven by genotype effects on early sessions, indicating that Ma2 activity might be involved in the planning/execution activity balance. Those results are now described in the results section and shown at the Supplemental Figure 4.

(4) For the experiments in which mice were trained prior to Ma2 cell activation (Fig.4), the behavior in sessions 8-10 does not seem to have reached a plateau yet, and the increase in successful prehensions in sessions 11-13 of Cre+ mice could just be a continuation of training. It would be more convincing to show the original training curve of those mice in sessions 1-7. Additionally, the authors should perform a two-way ANOVA test for the interaction of drug and genotype, rather than two separate one-way ANOVAs.

We agree, and we now show the curve for sessions 1-7 in Supplemental Figure 7, showing that the success ratio for sessions 8-10 is similar to session 7. Also, a 2-way ANOVA was already performed, although the full report was missing from the manuscript. We switched from successful prehensions per minute to success ratio (see Reviewer #1 comment 1a) and now include the full report, in which we found an overall effect of session, and when grouping by genotype, we found an effect for Cre+ but not control mice (lines 1065-1072).

Minor points

(1) The validation experiment for the efficacy of hM3Dq is somewhat confusing. It is surprising that the few hM3Dq-mCherry expressing cells in the cre-negative mice did not show increased c-Fos staining since non-specific leaky hM3Dq expression would presumably still lead to a functional DREADD. The better control for validating the efficacy of hM3Dq-mediated Chrna2-Cre cell activation would be to show c-Fos staining in Cre+ mice with or without clozapine injection. This would control for non-specific c-Fos expression and neuronal activation purely by expression of the DREADD. In cre-negative control mice, the comparison should also be between mice with and without clozapine injection to control for non-specific neuronal activation regardless of hM3Dq expression.

We thank the reviewer for raising this point and agree that validation of hM3Dq efficacy and specificity requires careful interpretation. In principle, any hM3Dq-expressing cell, including the few hM3Dq-mCherry+ cells observed in Cre- mice, could respond to clozapine. However, in practice, effective DREADD activation depends on sufficient receptor expression levels and on the pharmacodynamics of clozapine in the brain (Gomez et al., 2017, Science, 10.1126/science.aan2475). In our dataset, even in Chrna2-Cre+ mice, only ~76% of hM3Dq+ cells showed c-Fos induction after clozapine, indicating that receptor expression and/or

ligand access is not uniform across cells. Consistent with this, the very sparse and weak hM3Dq expression observed in Cre- mice resulted in only 0.8% of hM3Dq+ cells showing c-Fos induction, which is in line with previous reports demonstrating that low-level “leaky” expression is insufficient to drive neuronal activation (e.g. 10.1038/s41467-019-12236-z; 10.1523/JNEUROSCI.0537-18.2018; 10.1523/ENEURO.0363-21.2021).

The reviewer also suggests that an ideal validation would compare Cre+ mice with and without clozapine to control for any c-Fos induction driven purely by DREADD expression. We agree that such a comparison is informative, and note that in our experiments the c-Fos assay was designed specifically to test whether the low clozapine dose used (0.01 mg/kg) is sufficient to activate hM3Dq in Ma2 cells, rather than to assay baseline effects of viral expression.

Importantly, non-specific effects of clozapine itself were controlled for throughout the study by administering the same clozapine dose to both Chrna2-Cre+ and Cre- mice in all behavioral and physiological experiments. Thus, any clozapine-driven neuronal activation independent of hM3Dq would be expected to appear in both groups.

Together, these results indicate that (i) the clozapine dose used is sufficient to robustly activate hM3Dq-expressing Ma2 cells, (ii) sparse leaky expression in Cre- mice is not sufficient to drive measurable activation, and (iii) the effects reported in the manuscript are unlikely to be explained by non-specific clozapine actions or by viral expression alone.

(2) The authors state in the methods section that “only neurons that displayed a significant change comparing the before onset and after onset phases” were included in the analysis. This appears to bias the data towards neurons that change their activity with the prehension movement. If this is the intention, the authors should clearly state this and their rationale in the results section and show what proportion of recorded neurons fall into this category.

Yes, thanks for pointing this out, the explanation for this exclusion criteria is missing. We expanded the methods section “Neural activity around prehensions” to explain that since we are evaluating the role of Ma2 cells in the prehension-related activity of pyramidal cells, we excluded neurons with no prehension-related activity. We also stated in the expanded text that 15.97% of recorded neurons were excluded due to no prehension-related activity.

(3) I don't understand the peak PC activity latency shown in Figure 2D. How is it possible that there are negative peak latencies during the prehension phase, which is defined as >0sec, (upper right panel), and positive peak latencies in the before prehension phase, which is defined as <0sec, (lower right panel)?

As stated in lines 939-941 and in the figure 2C legend, neurons were sorted into “before prehension” or “during prehension” neurons according to their activity during the successful prehension. One of our main findings is that the pyramidal cells temporal patterns were strongly affected by prehension accuracy (lines 941-944) meaning that a significant number of neurons shifted prehension phases when performing a failed prehension (as illustrated in Figure 2C, note how the temporal pattern is not kept from successful to failed prehensions). That is why, for failed prehensions, there are negative latencies for neurons that were classified as “during prehension” and positive latencies for neurons classified as “before prehension” in successful trials. We expanded the sorting explanation in the results section (lines 944-950) to better highlight the latency change between different prehension accuracies.

(4) Please specify how baseline subtraction (detrrending) was performed for the calcium image analysis.

We expanded the methods section “Neural signal extraction” to better explain that we will now refer to F0 as the background component (and refer to our resulting traces as dF/F) and explain how it was determined (lines 614-619).

(5) The authors state that they found a "dissociation between changes in neural activity and performance outcomes". Since they only analyzed motor performance by quantifying successful prehensions, this statement should be caveated with the notion that other aspects of the behavior (e.g., trajectories/speed) could be affected but were not measured.

We agree, and expanded the discussion section to acknowledge that we focussed the behavioral aspects to success ratio, and that other measures not investigated could also be affected (lines ???-???).

(6) Are the differences in theta and gamma power specific to the prehension trials, or does Ma2 cell activation generally increase LFP activity in those bands?

We thank the reviewer for the question, as we had not analyzed general LFP activity in the previous version. We performed the same analysis now including only LFP from epochs outside prehension windows across the full sessions. We found that Ma2 cell activation actually reduces LFP power across all bands specifically in Session 13 when no prehension is being performed. These findings are now included as Supplemental Figure 7.

(7) Please define terms that might not be familiar to a typical reader in the field, such as "assemblies", when first introducing them in the text.

We revised the introduction where we now define assemblies (lines 85-88).

(8) Please specify the n-numbers for each figure throughout the manuscript. For example, in some figures, the number of trials or the number of neurons is used; however, it is not clear what this number is.

We agree that although the n-numbers are stated in the text, it would be clearer to add them also to the figure legends. All figure legends now contain n-numbers for panels showing quantifications.

(9) Relatedly, while the inclusion of supplemental tables with expanded statistical results is commendable, several statistical test details are missing, such as for Figure 5.

We have fully revised the text to add any missing statistical details for the statements in the Supplemental Tables.

<https://doi.org/10.7554/eLife.109286.2.sa0>